Available online at www.CivileJournal.org

Civil Engineering Journal

(E-ISSN: 2476-3055; ISSN: 2676-6957)

Vol. 11, No. 11, November, 2025

Enhancing AA6061–Bottom Ash Composites: Role of Heat Treatment on Properties and Dimensional Stability

Harjo Seputro [1], Sefrian R. Bintoro [2], Dody Ariawan [1], Eko Surojo [1], Triyono [1*]

[1] *Department of Mechanical Engineering, Universitas Sebelas Maret, Surakarta 57126, Indonesia.*

[2] *Department of Mechanical Engineering, Universitas Jenderal Soedirman, Purbalingga 53371, Indonesia.*

Received 20 August 2025; Revised 18 October 2025; Accepted 21 October 2025; Published 01 November 2025

Abstract

Aluminum matrix composites (AMCs) reinforced with industrial by-products have attracted attention as lightweight, sustainable materials, yet most research has focused on fly ash. The higher density of bottom ash compared to fly ash makes bottom ash suitable for use as reinforcement in AMC. This study investigates the combined effect of BA reinforcement (0, 3, and 6 wt%) and T6 heat treatment (aging at 175, 200, and 225 °C) on the microstructure, mechanical performance, thermal expansion, and dimensional stability of AA6061 composites. Mechanical testing, thermomechanical analysis (TMA), and coordinate measuring machine (CMM) evaluations were conducted to establish correlations between microstructure and macroscopic reliability. The results show that aging plays a decisive role in strengthening and stabilizing the alloy. The unreinforced AA6061 achieved peak hardness (69.43 BHN) and tensile strength (274.60 MPa) at 200 °C, but exhibited the largest distortion due to high thermal expansion. BA addition significantly reduced the mean coefficient of thermal expansion, with the 3 wt% BA composite aged at 200 °C demonstrating the most balanced behavior: stable CTE response, minimal distortion (0.1–0.4 mm²), and improved mechanical reliability. In contrast, 6 wt% BA composites, despite their lowest mean CTE (≈25 ppm/K), suffered from local instabilities due to particle agglomeration and porosity, leading to reduced toughness and higher geometric irregularities. Overall, this work highlights the novelty of employing BA as a sustainable reinforcement distinct from fly ash, showing that moderate BA addition coupled with optimized heat treatment can enhance dimensional stability and mechanical performance. The findings provide new insights into the design of cost-effective, environmentally friendly AMCs for structural applications.

Keywords: Aluminum Matrix Composite; Bottom Ash; Heat Treatment; Mechanical Properties; Dimensional Stability; TMA.

1. Introduction

Metal Matrix Composites (MMCs) have become increasingly important in civil and structural engineering applications due to their high strength-to-weight ratio, durability, and adaptability under demanding service conditions. These materials combine the toughness of metals with the hardness of ceramic reinforcements, resulting in superior performance in environments where mechanical reliability and reduced weight are essential. In infrastructure and construction, MMCs are being explored as substitutes for conventional alloys to reduce self-weight in load-bearing components, improve wear resistance in moving parts, and enhance thermal stability in high-temperature environments [1]. Such advancements are in line with the broader engineering goals of developing lightweight, sustainable, and long-lasting materials for modern construction systems.

Among various MMCs, Aluminum Matrix Composites (AMCs) have attracted significant attention owing to their low density, corrosion resistance, and promising mechanical behavior. Reinforcements such as Al_2O_3, SiC, and fly ash

* Corresponding author: triyono74@staff.uns.ac.id

http://dx.doi.org/10.28991/CEJ-2025-011-11-023

are often incorporated to improve strength, stiffness, and wear resistance [2–4]. Industrial-scale applications of AMCs demonstrate their potential not only in automotive and aerospace industries but also in civil engineering components such as brake drums, drive systems, and other load-transferring elements where dimensional stability and durability are critical [5]. Furthermore, the development of AMCs contributes to sustainable construction practices by reducing energy consumption through weight minimization and by utilizing industrial by-products as reinforcement materials.

A particularly relevant reinforcement in this context is coal bottom ash, an abundant industrial waste material produced in thermal power plants. In 2019, the United States generated approximately 30 million tons of coal fly ash and 9 million tons of bottom ash from coal-fueled power plants [6]. Bottom ash contains high levels of silica and alumina, making it suitable for use as a ceramic-like reinforcement in AMCs [7]. The higher density of bottom ash compared to fly ash makes bottom ash suitable for use as reinforcement in AMC. Unlike traditional ceramic particles, bottom ash offers the dual advantage of enhancing mechanical properties while contributing to waste management and circular economy strategies. The use of coal bottom ash as a reinforcement in AMC can improve mechanical properties such as strength, hardness, and wear resistance [8, 9]. Its reuse in composite fabrication not only reduces environmental burdens associated with ash disposal but also introduces cost-effective pathways for developing sustainable engineering materials [10].

Despite the promise of AMCs reinforced with industrial by-products, challenges remain in controlling their microstructure and dimensional stability under varying thermal conditions. The final performance of AMCs is determined not only by the type and distribution of reinforcement but also by subsequent post-processing, particularly heat treatment. Previous studies have shown that processes such as solution treatment, quenching, and artificial aging can substantially improve the strength and hardness of aluminum-based composites by purifying precipitates and improving interfacial bonding [11-14]. However, these treatments can also introduce residual stresses and distortion. Internal stresses generated during quenching or thermal exposure can cause irreversible dimensional changes in SiC/Al composites [15, 16]. This trade-off between mechanical enhancement and dimensional stability underscores the critical role of optimizing heat treatment for AMCs, particularly in structural and load-bearing applications where strength and geometric stability are critical.

Extensive studies have been conducted on the heat treatment of aluminum alloys and their dimensional stability in AMCs, with most research focusing on the properties of AMCs with various conventional reinforcements. The complex interactions between bottom ash fraction, heat treatment conditions, and dimensional behavior are not yet fully understood. Addressing these issues is crucial to ensure the mechanical performance and dimensional reliability of AMCs when applied in civil engineering systems and structures. Therefore, this study focuses on the effect of bottom ash addition and T6 heat treatment on the microstructural evolution, mechanical properties, and dimensional stability of AA6061-based composites. Particular emphasis is placed on testing the coefficient of thermal expansion (CTE), as dimensional stability under high temperature exposure is crucial for structural reliability. The next section describes the methodology and experimental procedures used, followed by a presentation of the main results and a discussion of them in the context of previous research. The article concludes with key conclusions and their implications for the development of sustainable and reliable aluminum composites using industrial waste-based reinforcements for civil engineering structural applications.

2. Materials and Methods

Aluminum Matrix Composites (AMCs) in this study were fabricated using AA6061 aluminum alloy as the matrix and bottom ash particles as the reinforcement. Prior to incorporation, the bottom ash underwent an electroless plating process to enhance interfacial bonding and improve wettability during stir casting. The reinforcement particles were prepared in a 300-mesh size, while magnesium powder, with a purity of 99.98% and particle size of 0.06–0.3 mm, was added as a wetting agent. The detailed compositions of the AMC constituents are presented in Tables 1 and 2, and three composite variations are listed in Table 3. A composition without additions (0%wt) was used as a control to compare the effects of bottom ash additions. 3%wt and 6%wt were used as medium-high composition parameters to explore the limits of property improvement because previous research ranges of 2-4% and 6%wt still provided improvements in mechanical properties and wear resistance [17, 18].

Table 1. Chemical composition of AA6061 (%wt)

Al	Mg	Si	Fe	Cu	Kr	Zn	Ti	Mn
95.85 - 98.56	0.8-1.2	0.40 -0.8	0.0-0.7	0.15 - 0.40	0.04 -0.35	0.0 -0.25	0.0 -0.25	0.0 - 0.15

Table 2. Chemical composition of coal bottom ash (%wt) [19]

SiO_2	Al_2O_3	Fe_2O_3	CaO	K_2O	TiO_2	MgO	P_2O_3	Na_2O	SO_2	BaO
42.7	23	17	9.8	0.96	1.64	1.54	1.04	0.29	1.22	0.19

Table 3.Composition of composites

Composite (%wt)	Composition		
	AA6061 (gram)	Bottom Ash (gram)	Mg (gram)
0% BA	2500	0	0
3% BA	2400	75	25
6% BA	2325	150	25

Fabrication was performed using the stir casting method, a widely applied liquid-phase technique for producing metal matrix composites. The AA6061 alloy was first melted in a melting furnace and then transferred to a holding furnace, where it was maintained at a temperature of 700–720 °C. The molten alloy was stirred using a four-blade impeller coated to resist corrosion, positioned at 30% of the crucible depth with a blade angle of 45°, and rotated at approximately 500 rpm to form a strong vortex as seen in Figure 1. Once the vortex stabilized, the pre-treated bottom ash particles were gradually added to the molten alloy. Stirring continued for 10 minutes to ensure uniform particle dispersion. To reduce hydrogen gas porosity and improve casting quality, Gas Bubble Filtration (GBF) was carried out using argon gas for approximately five minutes during stirring. The molten composite was then poured into preheated (500 °C) coated metal molds, with the pouring temperature maintained between 700–720 °C [20].

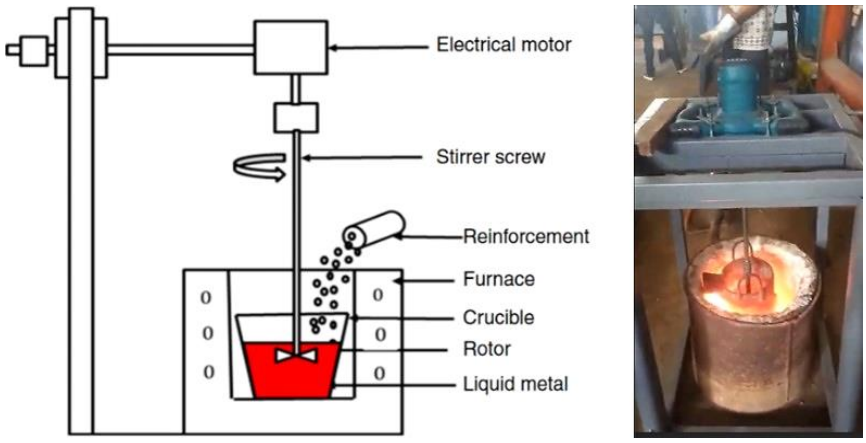

Figure 1. Stir casting process (a) schematic [21], (b) actual process

Following solidification, specimens were subjected to a T6 heat treatment to enhance their mechanical properties. The process was conducted using a Marvel Thermolyne Furnace (Model 30400) and involved three stages. First, a solution treatment was carried out at 540 °C for 6 h, followed by immediate water quenching. Subsequently, artificial aging was performed at temperatures of 175 °C, 200 °C, and 225 °C for 8 h [22], with final cooling in air. The complete heat treatment parameters are presented in Table 4.

Table 4. Heat treatment T6 with different artificial aging temperature

No.	Heat Treatment T6	
	Solution treatment	Artificial aging
1	Heating 540°C for 6 hours, followed by rapid quenching in water	Temperature of 175°C, holding time 8 hours
2	Heating 540°C for 6 hours, followed by rapid quenching in water	Temperature of 200°C, holding time 8 hours
3	Heating 540°C for 6 hours, followed by rapid quenching in water	Temperature of 225°C, holding time 8 hours

Mechanical properties were evaluated through hardness, tensile, and impact testing. Hardness tests were conducted in accordance with ASTM E10 using a Shimadzu Type-HB No. 8091 Brinell hardness tester with a 2.5 mm steel ball indenter, a load of 62.5 kgf, and a dwell time of 30 seconds. Three indentations were made at different points on each specimen as illustrated in Figure 2. Tensile tests followed ASTM E8 using a Universal Testing Machine at a crosshead speed of 10 mm/min. Figure 3 shows the geometry and dimension of tensile test specimen. Impact tests were carried out using the Charpy method according to ASTM E23 with a Shimadzu Type-CH No. 88919 machine, using specimens measuring 10 × 55 mm with a 45° notch as seen in Figure 4.

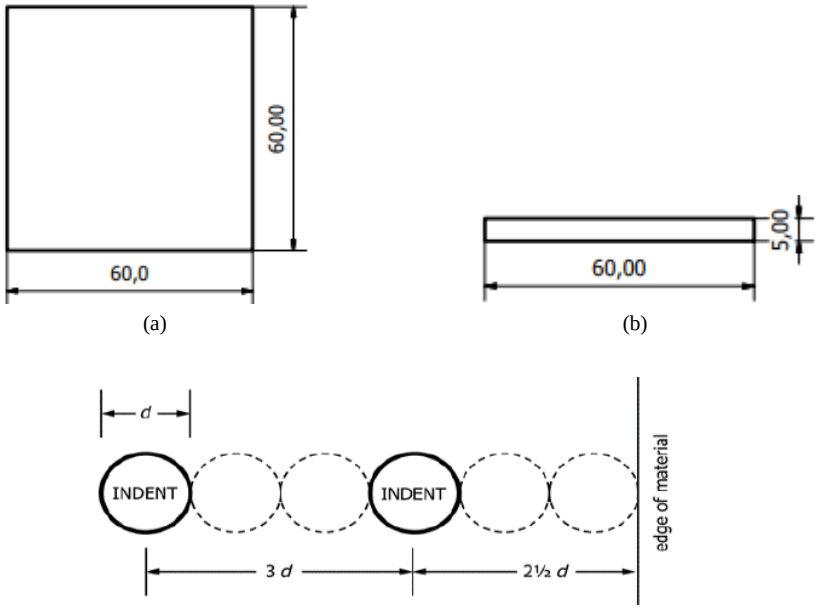

Figure 2. The hardness test specimen geometry (unit in mm): (a) top view, (b) side view, (c) distance between indentations

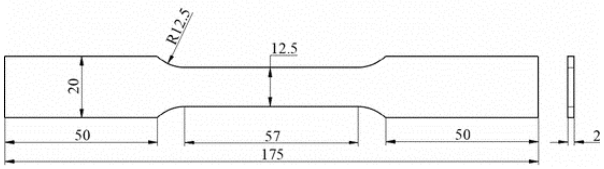

Figure 3. The tensile test specimen (unit in mm)

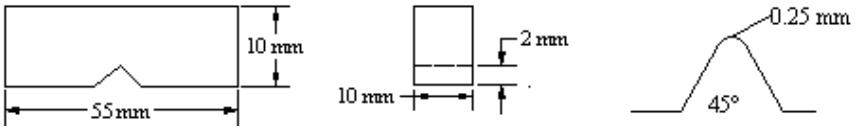

Figure 4. The impact test specimen (unit in mm)

Microstructural characterization was performed using optical microscopy and scanning electron microscopy equipped with energy-dispersive X-ray spectroscopy (SEM-EDX) to observe grain structure, particle dispersion, and the matrix–reinforcement interface. Figure 5 shows the SEM-EDX specimen geometry. Metallographic preparation involved grinding, polishing, and etching with Keller's reagent (2 mL HF, 3 mL HCl, 5 mL HNO_3 , and 190 mL distilled water) in accordance with ASTM E407. SEM-EDX observations were also carried out on fracture surfaces obtained from mechanical testing to analyze morphology and failure mechanisms.

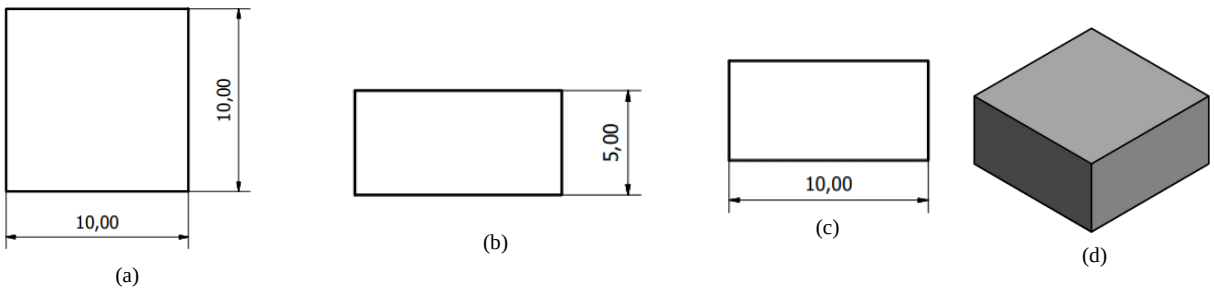

Figure 5. The SEM-EDX specimen geometry (unit in mm): (a) top view, (b) front view, (c) side view, (d) isometric

Dimensional stability was evaluated through thermal expansion testing and coordinate measurement. Thermal expansion tests followed ASTM E831 using a Thermomechanical Analyzer (TMA). Specimens (Figure 6) were placed in contact with the detection rod, and changes in length (ΔL) during heating were recorded by a Linear Variable

Differential Transformer (LVDT) to determine dimensional change with temperature (ΔT). Coordinate measurements were conducted using a Mitutoyo Bright 707 Coordinate Measuring Machine (CMM), which determines the three-dimensional positions of surface points with high accuracy. Specimen geometry and points of measurement of the CMM test are shown in Figure 7 while the process of measurement using CMM is displayed in Figure 8. The outline of this research is shown in Figure 9.

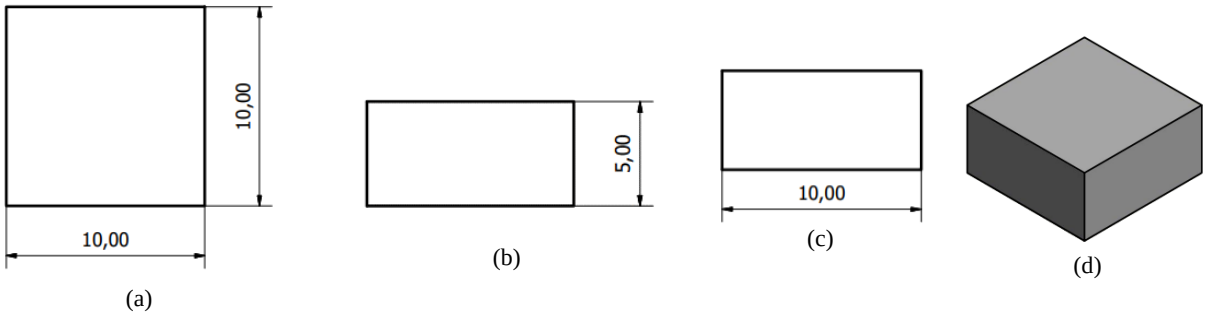

Figure 6. The thermal expansion test specimen (unit in mm): (a) top view, (b) front view, (c) side view, (d) isometric

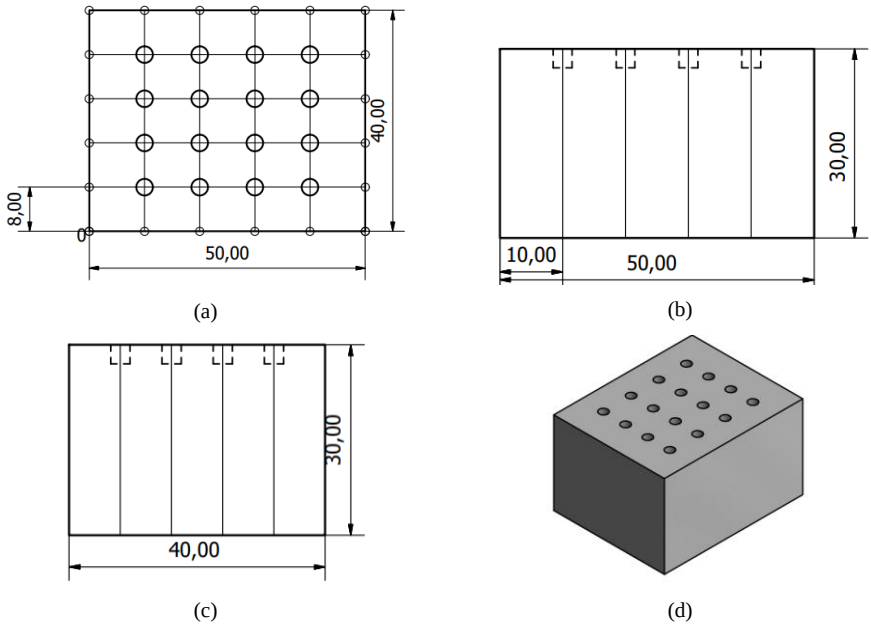

Figure 7. The CMM test specimen (unit in mm): (a) top view, (b) front view, (c) side view, (d) isometric

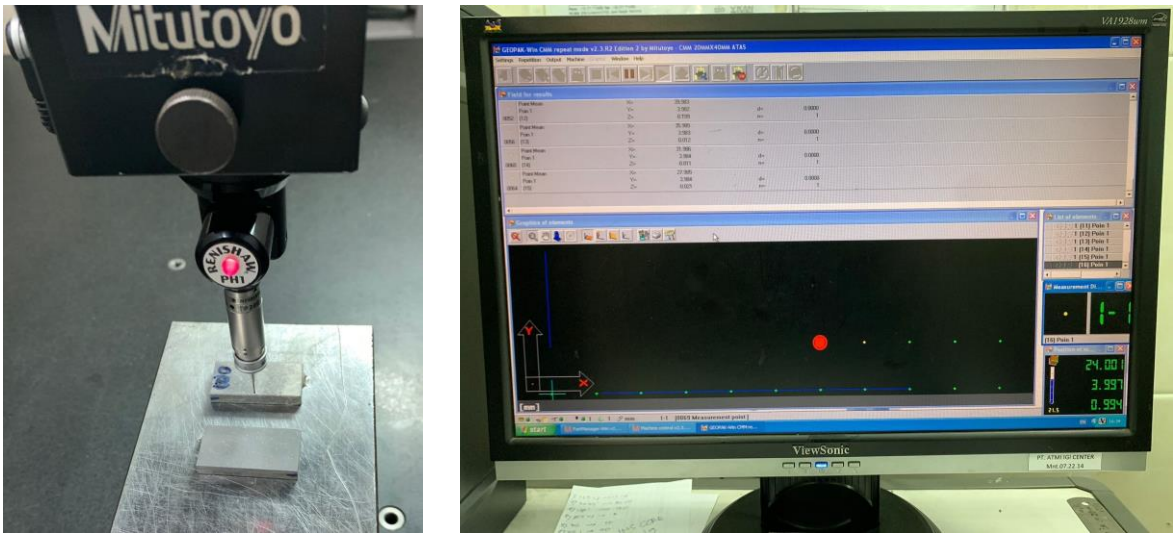

Figure 8. Process of CMM test (a) probe and specimen position, (b) monitor display

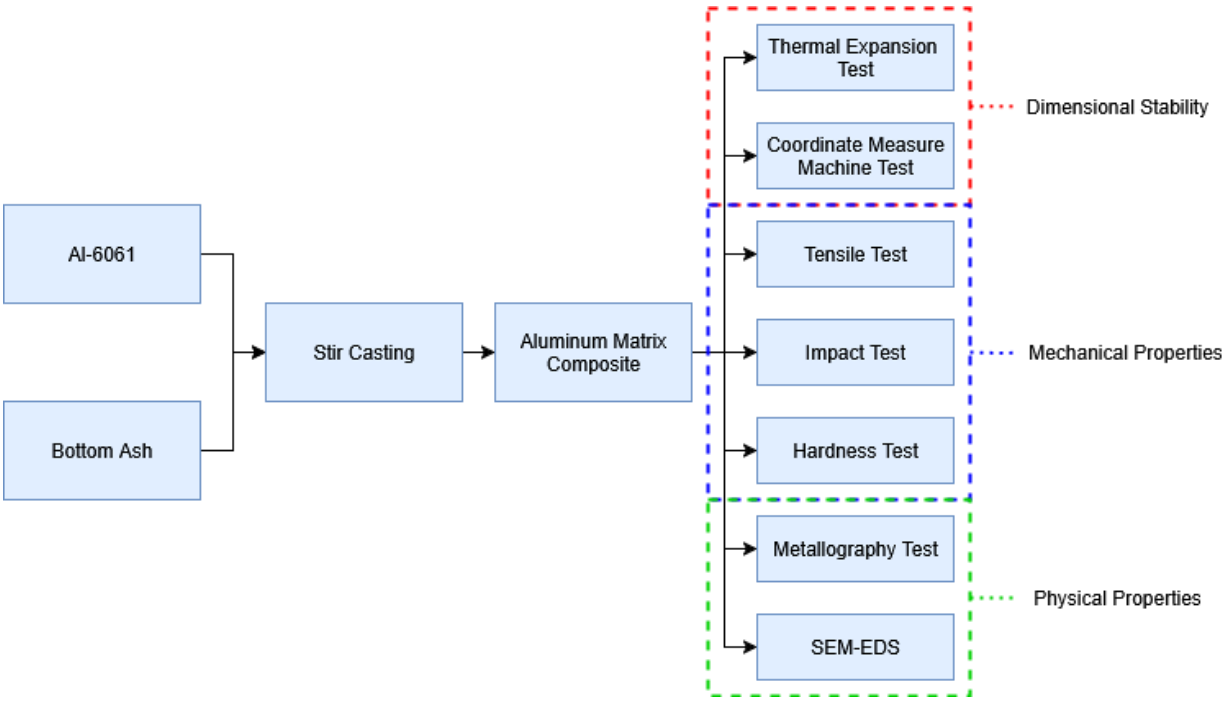

Figure 9. Research Methodology Flowchart

3. Results and Discussion

3.1. Density and Porosity

The evaluation of density and porosity provides essential insight into the structural integrity, homogeneity, and defect characteristics of aluminum matrix composites reinforced with bottom ash (AMC-BA). As shown in Figure 10, the density of the composites decreased progressively with increasing BA content. The theoretical density of AA6061 alloy is 2.698 g/cm³, while the measured density of the unreinforced matrix (0 wt% BA) was slightly lower, at 2.607 g/cm³. With the addition of 3 wt% and 6 wt% BA, the density further decreased to 2.596 g/cm³ and 2.574 g/cm³, respectively. This reduction can be attributed to two main factors. First, bottom ash possesses a lower intrinsic density (~2.53 g/cm³), which naturally reduces the overall density of the composite when incorporated as a reinforcement. Second, the porous and heterogeneous nature of BA particles increases the likelihood of entrapped voids during mixing and solidification, especially when particle wetting by the molten matrix is incomplete. This phenomenon has also been reported in aluminum–fly ash composites, where reinforcement with low-density and porous particulates consistently leads to a reduction in composite density [23, 24].

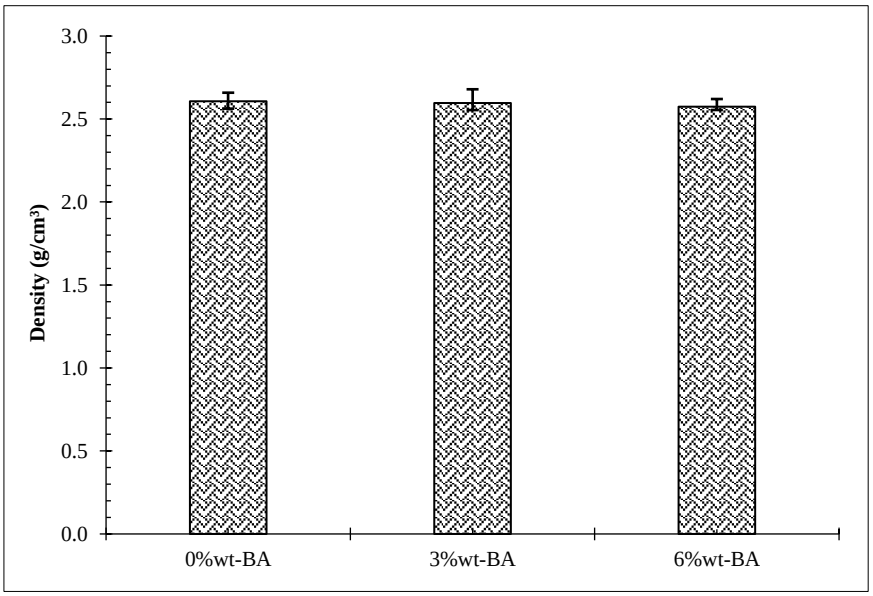

Figure 10. Density of AMC reinforced by bottom ash (BA)

The porosity observation results presented in Figure 11 further support this interpretation. The specimen reinforced with 6 wt% BA exhibited the highest porosity, reaching 3.7%, suggesting that excessive addition of BA promotes the formation of micro-voids and interfacial defects. Such defects are often associated with particle clustering, increased interfacial area, and inadequate matrix–particle bonding. Conversely, the composite containing 3 wt% BA demonstrated a lower porosity level (3.12%) [25], indicating more effective dispersion and improved particle–matrix interactions at this reinforcement level. A similar trend has been observed in studies on aluminum–fly ash composites, where moderate reinforcement contents resulted in relatively uniform microstructures and minimized porosity, while higher loadings caused agglomeration and defect formation [26-28]. Since porosity directly influences the strength and reliability of metal matrix composites, controlling its formation is critical to achieving desirable mechanical performance [29, 30].

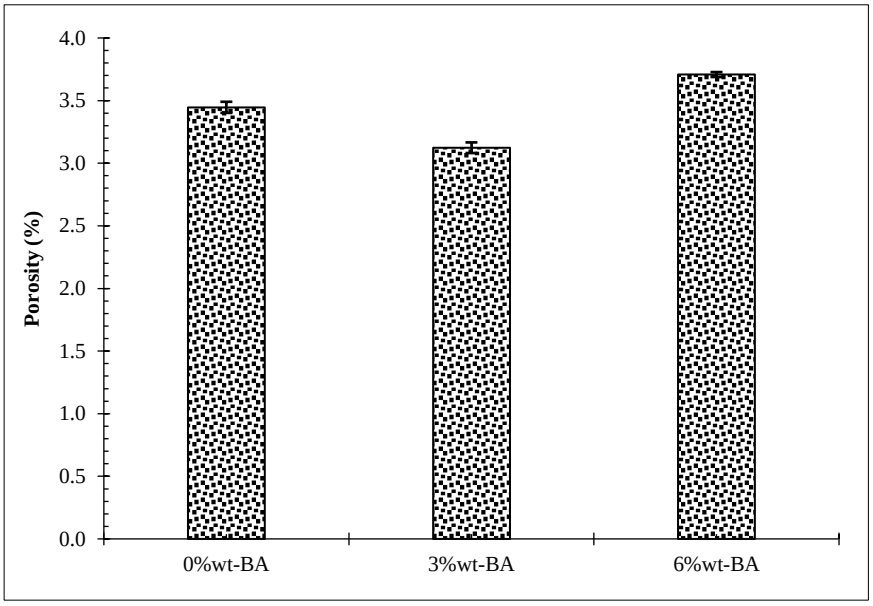

Figure 11. Porosity of AMC reinforced by bottom ash (BA)

Taken together, these findings highlight the importance of optimizing BA content in AMC systems. The addition of 3 wt% BA appears to provide the best balance, offering effective reinforcement without inducing excessive porosity that would compromise structural performance. At this concentration, the composite maintains satisfactory density while exhibiting reduced porosity compared to both the unreinforced matrix and the higher BA loading. This suggests that 3 wt% BA is an optimal threshold, enabling improved performance alongside the added benefits of cost reduction and sustainability by utilizing industrial waste. However, reinforcement contents beyond this level may diminish the advantages due to increased porosity and weak interfacial bonding, which ultimately reduce the mechanical stability of the composite.

These results are consistent with broader research on the use of industrial by-products such as fly ash and bottom ash in aluminum composites. Previous studies have emphasized that incorporating small amounts of these reinforcements can enhance properties while promoting sustainable materials development, but excessive contents often lead to porosity, poor wettability, and clustering [26, 29, 30]. Thus, the present findings reinforce the critical need for process optimization to maximize the potential of bottom ash as a cost-effective and eco-friendly reinforcement in aluminum matrix composites.

3.2. Metallography Observation

The SEM-EDS analysis of bottom ash (BA) particles (Figure 12 and Table 5) revealed dominant elements such as O, Si, Al, Ca, C, and S, indicating the presence of oxides including SiO_2 , Al_2O_3 , CaO, and SO_3 . These compounds are consistent with the ceramic-rich composition of BA, which is generally regarded as inert, hard, and resistant to abrasion [19]. Among them, Al_2O_3 and SiO_2 are particularly noteworthy since both are commonly employed reinforcements in aluminum matrix composites (AMCs), and their addition has been shown to enhance hardness, wear resistance, and load-bearing capacity [31, 32]. This chemical profile suggests that BA has the potential to act as a cost-effective reinforcement, similar to fly ash, which has been widely investigated as a ceramic-rich byproduct for AMC development [23, 24].

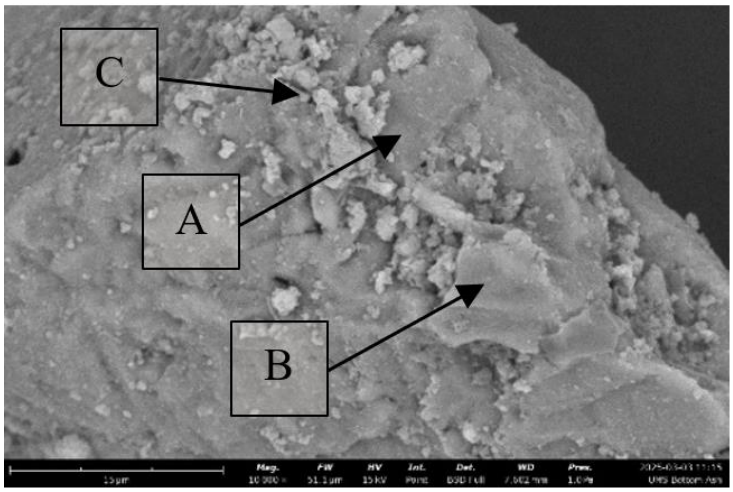

Figure 12. SEM of bottom ash (BA)

Table 5. EDS of bottom ash

Point	Element Number	Element symbol	Element Name	Atomic Conc. (%)	Weight Conc. (%)
Point A	6	C	Carbon	33.579	23.4
	8	O	Oxygen	45.132	41.9
	14	Si	Silicon	21.29	34.7
Point B	6	C	Carbon	31.64	21.8
	8	O	Oxygen	46.083	42.3
	14	Si	Silicon	22.277	35.9
Point C	6	C	Carbon	19.267	12.4
	8	O	Oxygen	58.199	49.9
	13	Al	Aluminum	3.044	4.4
	14	Si	Silicon	11.493	17.3
	16	S	Sulfur	2.735	4.7
	20	Ca	Calcium	5.261	11.3

The microstructural evolution of the composites was strongly influenced by both heat treatment and reinforcement content (Figure 13). In the unreinforced alloy (0 wt%–T0), the structure was dominated by coarse and non-uniform α-Al grains, reflecting the as-cast condition with minimal precipitation. Application of T6 heat treatment led to a significant refinement of grains, particularly at an aging temperature of 175 °C, where a more uniform distribution of fine precipitates was observed. At 200 °C, secondary precipitates were more distinctly distributed along grain boundaries, enhancing microstructural uniformity.

However, at higher temperatures (225 °C), overaging occurred, characterized by precipitate coarsening and reduced dislocation hindrance, which in turn compromised mechanical strength. These observations align with prior findings showing that AA6xxx-series alloys exhibit strong sensitivity to aging temperature and duration: fine, coherent precipitates formed under optimal conditions (e.g., T6 treatment) enhance strength, whereas extended or higher-temperature aging causes precipitate coarsening and significant mechanical degradation [33] on AA6061 overaging), supported by data showing that artificial aging between 160–220 °C critically governs precipitation kinetics and final properties in AA6xxx alloys [34, 35], and corroborated by comprehensive reviews on the distinction between T6 (peak-hardened) and T7 (over-aged) conditions in aluminum alloys.


100 µm

(a)

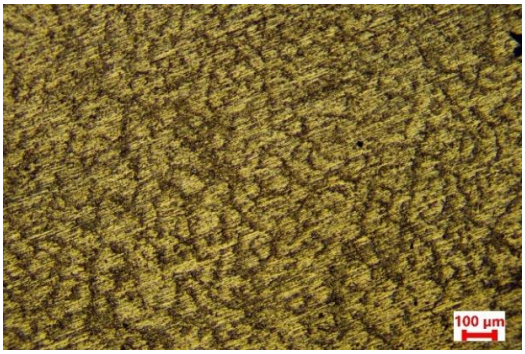
100 µm

(b)

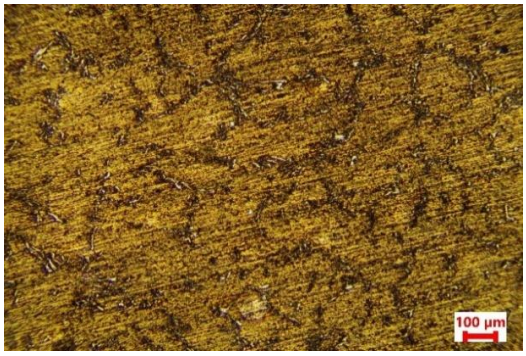
100 µm

(c)

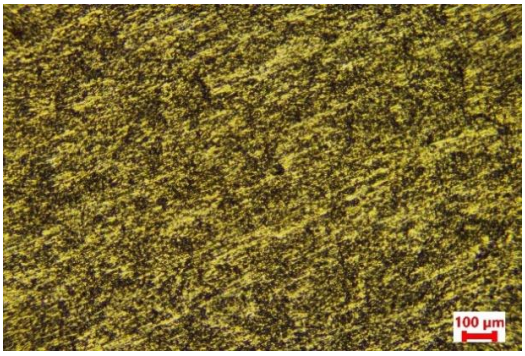
100 µm

(d)

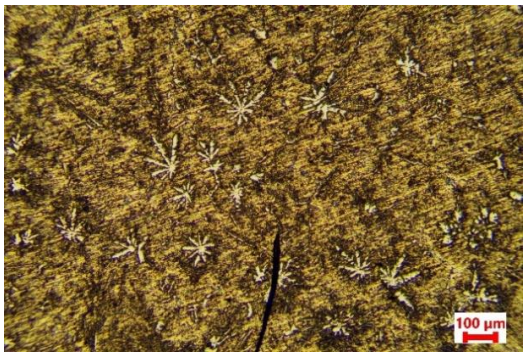
100 µm

(e)

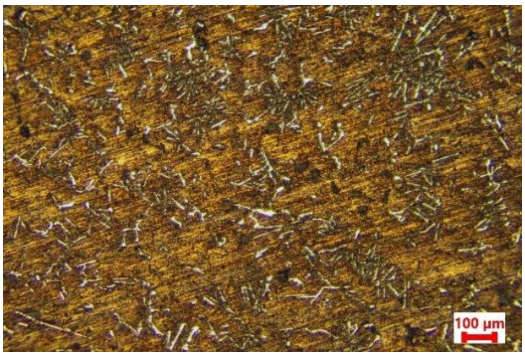
100 µm

(f)

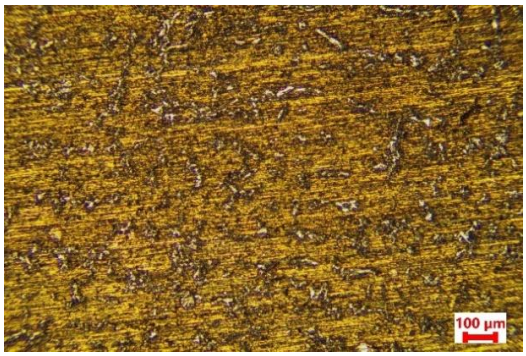
100 µm

(g)

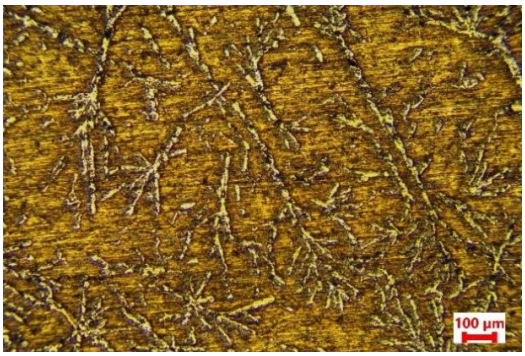
100 µm

(h)

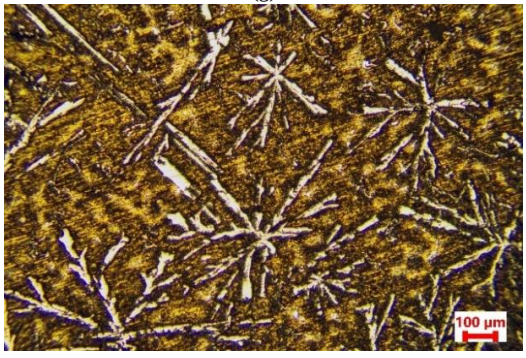
100 µm

(i)


100 µm

(j)

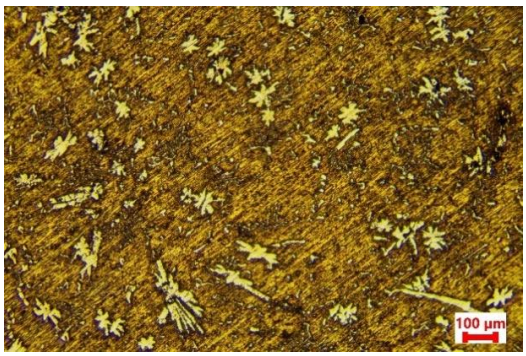

(k)

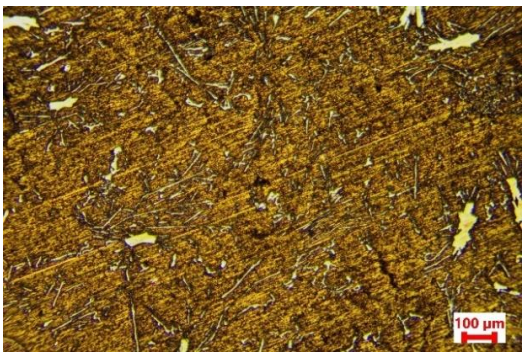

(l)

Figure 13. Microstructure of Al6061-BA (a). 0%wt-T0; (b). 0%wt-T175; (c). 0%wt-T200; (d). 0%-T225; (e). 3%wt-T0; (f). 3%wt-T175; (g). 3%wt-T200; (h). 3%wt-T225; (i). 6%wt-T0; (j). 6%wt-T175; (k). 6%wt-T200; (l). 6%wt-T225

When BA was introduced at 3 wt%, the microstructure displayed reinforcement particles with a dendritic morphology and non-uniform distribution in the unaged condition. After aging at 175 °C, however, the dispersion of BA particles improved, with reinforcement phases appearing along grain boundaries. This suggests that BA particles contributed to a grain boundary pinning effect, which helped to stabilize grain size. At 200 °C, the microstructure became more refined, with secondary precipitates and BA particles distributed more evenly, some aligned in the direction of flow during casting. This condition can be considered near-optimal, as both the precipitate structure and reinforcement distribution were favorable for strengthening. Similar behavior has been reported in stir-cast Al6061 composites reinforced with fly ash and ceramic particles. For instance, a hybrid composite of AA6061 with $Al_2 O_3$ and fly ash showed improved tensile strength (up to ~175 MPa) and uniform reinforcement dispersion after heat treatment [36]. Another study involving Al6061-T6 reinforced with fly ash and graphite produced composites free from porosity and improved yield strength [37]. A broader review also supports that fly ash can enhance tensile, compressive, and hardness properties by promoting refined microstructures when optimally dispersed [38].

In contrast, the addition of 6 wt% BA introduced significant heterogeneity. Without heat treatment, BA particles tended to cluster, reflecting poor dispersion during mixing. Aging treatments partially improved the distribution of precipitates but could not eliminate BA agglomeration, which remained prominent. At 225 °C, overaging intensified, with coarser precipitates, larger inter-precipitate spacing, and more pronounced BA clustering. These defects are critical because they promote localized weaknesses and higher porosity, which ultimately diminish the composite's mechanical reliability. Comparable trends have been observed in Al–fly cream composites: as reinforcement content increases beyond an optimal threshold, porosity increases and particle agglomeration occurs, leading to impaired structural integrity (AA6063–fly ash: rising porosity and agglomeration with fly ash content [29]; ADC10–fly ash: higher fly ash content decreasing mechanical strength due to porosity [24]; AA6061 stir-cast MMCs: reinforcement beyond a limit causes clustering and porosity [30]; high reinforcement hybrid MMCs: agglomeration induces crack initiation and ductility loss [39].

Another significant feature identified in both BA-reinforced and unreinforced composites was the presence of acicular Al_5 FeSi intermetallic phases, which became more pronounced with increasing BA content. The high Si and oxide content of BA likely accelerated the formation of Fe-rich intermetallics such as β-Al_5 FeSi. While limited and well-distributed intermetallics can contribute to strengthening, excessive or elongated morphologies, especially plate-like or needle-shaped β-Al_5 FeSi, act as stress concentrators and promote brittleness. This effect has been documented in recycled Al alloys, where sharp β-Al_5 FeSi needles initiated micro-cracks [40] and, more broadly, where brittle intermetallics with unfavorable morphology triggered crack propagation along particle-matrix boundaries, undermining mechanical reliability [41]. Taken together, these results indicate that the microstructure of AA6061–BA composites is jointly governed by reinforcement content and heat treatment conditions. The best balance was obtained with 3 wt% BA aged at 200 °C, where grain refinement, uniform precipitate distribution, and effective reinforcement dispersion combined to yield a stable microstructure. By contrast, excessive BA content (6 wt%) or overaging at 225 °C both led to structural heterogeneity, precipitate coarsening, and reinforcement agglomeration, ultimately reducing mechanical performance. These findings align with broader literature on AMCs reinforced with fly ash and similar byproducts, underscoring the necessity of optimizing both reinforcement fraction and thermal treatment to achieve the desired balance between strength, ductility, and reliability.

3.3. Hardness

The Brinell hardness results (Figure 14) clearly demonstrate the strong influence of aging and reinforcement on composite hardness. The lowest hardness (32.67 BHN) was observed in the unreinforced and unaged condition (0 wt%–T0), whereas the highest hardness value (69.43 BHN) occurred in the unreinforced alloy aged at 225 °C (0 wt%–T225). This significant enhancement confirms that T6 heat treatment substantially increases hardness in the pure aluminum

matrix, largely due to the precipitation hardening of Mg_2 Si acting as effective dislocation barriers. Such behavior echoes findings in AA6xxx alloys, where aging leads to peak hardness, while extended aging (overaging) results in hardness reduction due to precipitate coarsening and loss of dislocation impediments [42].

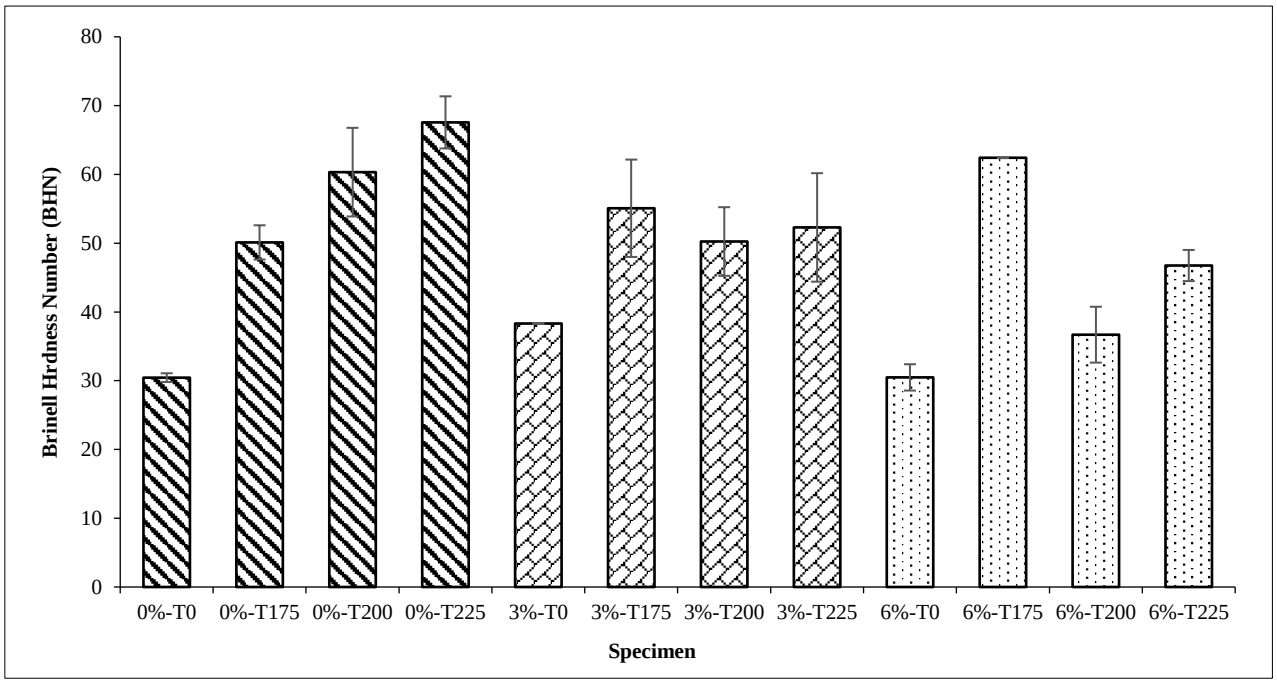

Figure 14. Hardness of AA6061–BA composites

A similar trend was observed in the BA 3 wt% reinforced composite. Without aging, the hardness remained low, but aging at progressive temperatures increased the hardness. However, the maximum hardness was still less than that of the unreinforced T225 condition. This indicates that BA contributes to hardening through additional mechanisms, namely load transfer and the Orowan effect when the interparticle spacing is sufficiently close. Thus, the hardness increase stems not only from Mg_2 Si precipitation but also from the role of reinforcing particles. The reinforcing effect of BA works synergistically with Mg_2 Si precipitation, increasing hardness, but its efficacy depends on the aging temperature and particle distribution. These results align with previous research where ceramic reinforcement dispersions in aluminum alloys can synergistically increase hardness with precipitation. However, with 3 wt% BA, the peak hardness is reached at a lower aging temperature than with the pure alloy, indicating possible accelerated precipitation around the BA interface due to local stress gradients [43-45].

In the 6 wt% BA series, the highest hardness is achieved at 175°C (61.63 BHN), while higher aging temperatures lead to a decrease in hardness. This phenomenon indicates a tendency for accelerated overaging. Two main factors can explain this: (i) the Mg_2 Si precipitates become coarse and lose their effectiveness in inhibiting dislocations, and (ii) the agglomeration and inhomogeneous distribution of BA lead to the formation of local zones of high stress concentration. This condition reduces the uniformity of the hardening response. This is consistent with a common observation in Al-Mg-Si systems: peak hardness occurs at a certain aging temperature, and after that point, the hardness decreases due to coarsening of the precipitates [42]. The role of heat treatment is crucial in tuning the hardness of composites. Optimization of aging should be tailored to the reinforcement fraction: unaged specimens exhibit low hardness due to a coarse microstructure, large grains, and undeveloped Mg_2 Si precipitates. Furthermore, the porosity inherent in the as-cast process further compromises hardness. In the pure alloy, the apparent increase in hardness at T225 is most likely due to precipitates hardening at grain boundaries, although this can lead to brittleness and reduced toughness—as observed in previous tensile tests. In the 3 wt%–T225 variant, over-aging becomes evident through enlarged precipitates and reduced dislocation inhibition, although BA still contributes to a stiffer response [46].

The 6 wt% BA composites present a more complex scenario: while aging increases hardness, structural flaws such as reinforcement clustering and inhomogeneous distribution, most severe without aging, limit performance. Partial diffusion or dissolution of BA particles may contribute, but uneven dispersion impairs the uniformity of mechanical improvements. At 225 °C, overaging appears in all composites, with hardness gains via growth of hard phases, but at the cost of significantly reduced ductility and possibly increased brittleness. In sum, composites with finer intermetallic phases generally show higher hardness, yet a delicate balance must be maintained to prevent mechanical degradation [47, 48].

3.4. Tensile Strength

In the as-cast (T0) condition, the ultimate tensile strength (UTS) only reached 102.67 MPa, as shown in Figure 15. This relatively low value reflects the presence of a coarse microstructure with large grains and the absence of significant strengthening precipitates. However, after aging heat treatment at 175 °C, the UTS increased drastically to 256.20 MPa. This improvement can be attributed to the formation of fine Mg_2 Si precipitates, which strengthen the aluminum matrix through the precipitation hardening mechanism. Similar findings have been reported for Al–Mg–Si alloys, where peak strength is typically achieved at aging temperatures around 170–180 °C due to the formation of β″ precipitates that effectively hinder dislocation motion without sacrificing ductility [42, 49].

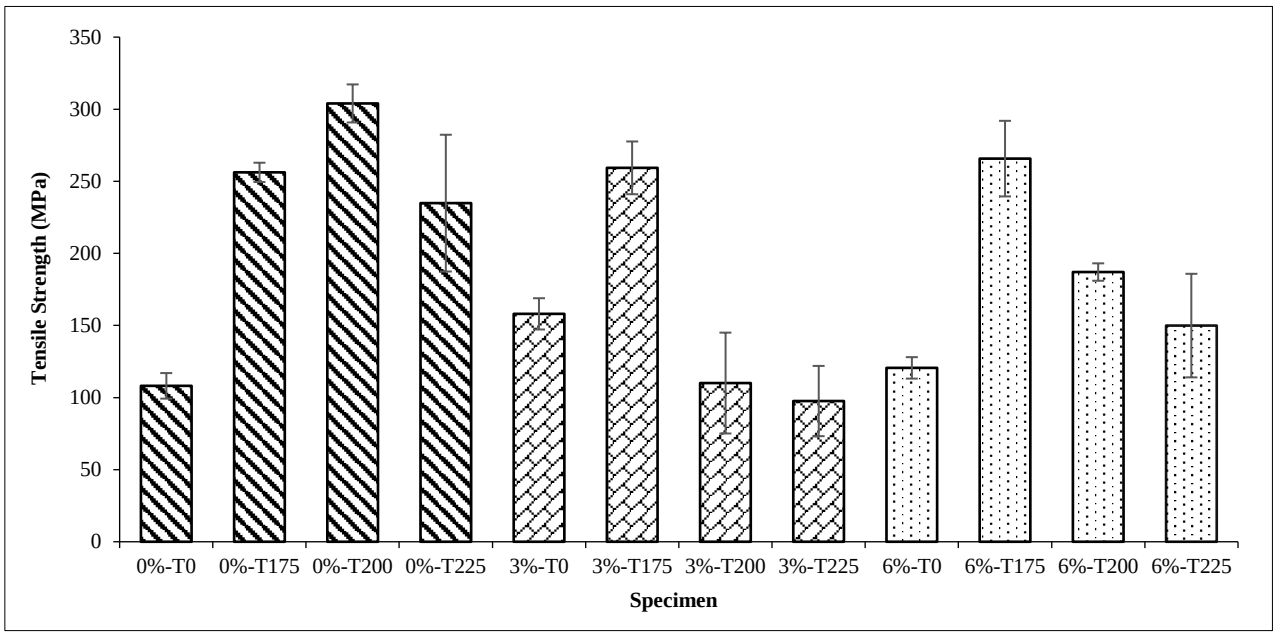

Figure 15. Tensile strength of AA6061–BA composites

The peak strengthening effect was observed at an aging temperature of 200 °C, with the highest UTS of 274.60 MPa. At this stage, the size and distribution of precipitates are in their optimum condition (peak aging), thereby effectively impeding dislocation motion. However, when the aging temperature was increased to 225 °C, the UTS dropped to 234.87 MPa, indicating an overaged condition. Overaging occurs when precipitates coarsen, thereby reducing their effectiveness as dislocation barriers. This behavior is well-documented in precipitation-hardened Al–Mg–Si alloys, where excessive aging leads to significant loss of tensile strength [44, 45].

The addition of 3 wt% BA particles in the T0 condition increased the UTS to 146.09 MPa. This enhancement indicates the particle reinforcement effect of BA, despite the microstructure still being in the as-cast state. However, the measured elongation remained relatively low (5.47%), suggesting that although BA improved strength, it did not significantly enhance ductility. After heat treatment at 175 °C, the UTS further increased to 259.33 MPa. This improvement can be attributed to the combined effect of BA particle reinforcement and Mg_2Si precipitation strengthening, consistent with the synergistic strengthening mechanisms observed in particle-reinforced aluminum composites [49, 50]. Interestingly, when aging was carried out at 200 °C, the UTS dropped to 197.53 MPa. This reduction is likely caused by negative interactions between precipitates and BA particles, such as particle agglomeration or interference with precipitate growth. A more drastic decline occurred at 225 °C (UTS = 97.60 MPa), indicating that overaging, coupled with increased porosity, dominated the mechanical behavior of the composite. Moreover, the interfaces between BA particles and the aluminum matrix may accelerate Mg and Si diffusion, leading to faster precipitate coarsening in localized regions and causing premature overaging. In addition, residual stresses arising from the coefficient of thermal expansion mismatch between BA and the matrix generate stress concentrations at the interfaces, which promote microcrack initiation. These combined effects explain why the 3 wt% BA composite loses strength at 200 °C while the unreinforced alloy shows improvement.

The addition of 6 wt% BA showed a more complex trend. In the T0 condition, the UTS was 130.04 MPa. Although more reinforcement particles were present, particle agglomeration and porosity hindered effective strengthening [47]. After heat treatment at 175 °C, the tensile performance significantly improved, with UTS reaching 265.73 MPa, suggesting that effective precipitation occurred even in the presence of BA particles. However, the UTS decreased again at 200 °C (180.71 MPa) and further at 225 °C (149.93 MPa). This decline is likely caused by the combined effects of overaging, particle agglomeration, and porosity, which disrupt matrix continuity and act as crack initiation sites during deformation [51, 52].

Furthermore, it is noteworthy that the decrease in strength in the 3 wt% BA composite tested at 200°C, while the unreinforced alloy showed an increase, can be explained by a more complex microstructural interaction mechanism. At this temperature, Mg_2Si precipitation in the pure alloy is still near its peak aging state, resulting in peak strength. However, in composites, the interface between BA particles and the aluminum matrix can accelerate the diffusion of Mg and Si atoms around the particles, causing precipitates to grow more rapidly in these zones. This results in local overaging in the area around the BA particles. Although the overall aging temperature still supports strengthening, some microstructure regions lose the effectiveness of fine precipitates. This phenomenon is exacerbated by residual stresses resulting from the thermal mismatch between BA and the matrix, which triggers local stress concentrations and accelerates crack initiation [16].

The distribution of the Al_5FeSi intermetallic phase also significantly affects tensile strength. A fine and short distribution of Al_5FeSi (e.g., in the 0 wt%–T200 or 3 wt%–T175 specimens) increases strength by inhibiting dislocation motion. Conversely, coarse and sharp Al_5FeSi phases (as observed in the 6 wt%–T200 or 6 wt%–T225 specimens) serve as crack initiation sites, substantially reducing tensile strength. Tensile strength testing confirmed that the aging heat treatment plays a decisive role in determining the mechanical performance of the composite. In the pure alloy, 200 °C yielded the highest strength because the precipitates were at their optimum state. However, for the 3–6 wt% BA composite, the best condition was achieved at 175 °C, because at this temperature the combination of fine precipitates, relatively homogeneous BA particles, combined with short, evenly distributed Al_5FeSi phases as seen on the fracture surface in Figure 16 and the EDS results (Table 6), effectively inhibited dislocation motion without creating severe stress concentrations. This observation is consistent with previous studies emphasizing the important role of controlled precipitation and microstructural refinement in optimizing the strength-ductility balance of aluminum composites [49, 50].

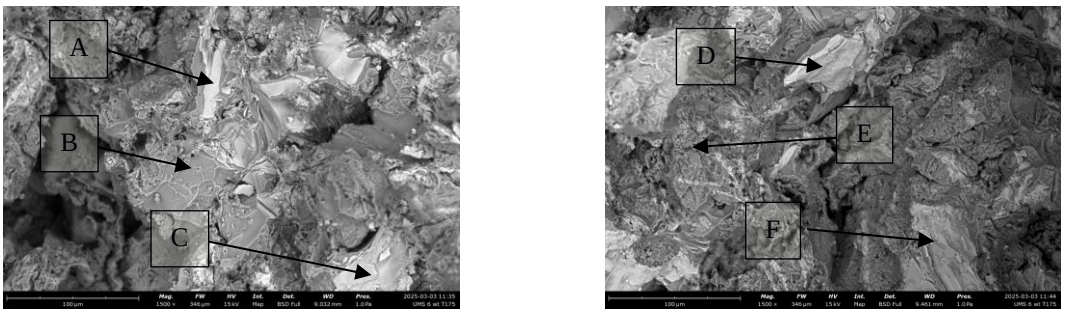

Figure 16. SEM on the surface fracture of 3 wt%–T175 specimen

Table 6. EDS on the fracture of 3 wt%–T175 specimen

Point	Element Number	Element symbol	Element Name	Atomic Conc. (%)	Weight Conc. (%)
Point A	6	C	Carbon	17.349	7.293
	13	O	Oxygen	62.758	59.241
	14	Si	Silicon	5.487	5.395
	24	Cr	Chromium	0.659	1.199
	26	Fe	Iron	13.747	26.873
Point B	13	Al	Aluminum	100.000	100.000
Point C	8	C	Oxygen	1.184	0.601
	13	O	Aluminum	75.170	64.264
	14	Si	Silicon	7.644	6.807
	26	Fe	Iron	16.001	28.328
Point D	6	C	Carbon	10.897	4.400
	13	Al	Aluminum	68.048	61.700
	14	Si	Silicon	6.036	5.700
	26	Fe	Iron	15.019	28.200
Point E	8	O	Oxygen	3.980	2.400
	13	Al	Aluminum	96.020	97.600
Point F	6	C	Carbon	17.209	7.207
	13	Al	Aluminum	62.266	58.559
	14	Si	Silicon	5.927	5.806
	26	Fe	Iron	14.597	28.428

3.5. Impact Strength

Impact testing was carried out to evaluate the ability of the material to absorb energy before experiencing sudden fracture, expressed as specific energy absorption (J/mm²). The results of impact testing as seen in Figure 17 indicate that the impact toughness of the composites is strongly influenced by microstructure, porosity, precipitation behavior, and the distribution of bottom ash (BA) reinforcement particles. For the unreinforced alloy (0 wt% BA) in the as-cast (T0) condition, the specific absorbed energy was 0.0207 J/mm². After T6 heat treatment at an aging temperature of 175 °C, the impact strength increased significantly to 0.0681 J/mm². This improvement is attributed to the formation of fine, homogeneously distributed Mg_2Si precipitates, which strengthen the matrix while retaining adequate ductility. However, with further aging at 200 °C and 225 °C, the impact strength decreased to 0.0543 J/mm² and 0.0515 J/mm², respectively. This decline reflects the onset of overaging, where precipitates coarsen and lose their ability to enhance toughness effectively. Such behavior has been widely reported in Al–Mg–Si alloys, where excessive precipitation growth leads to embrittlement and reduced impact energy absorption [4, 49].

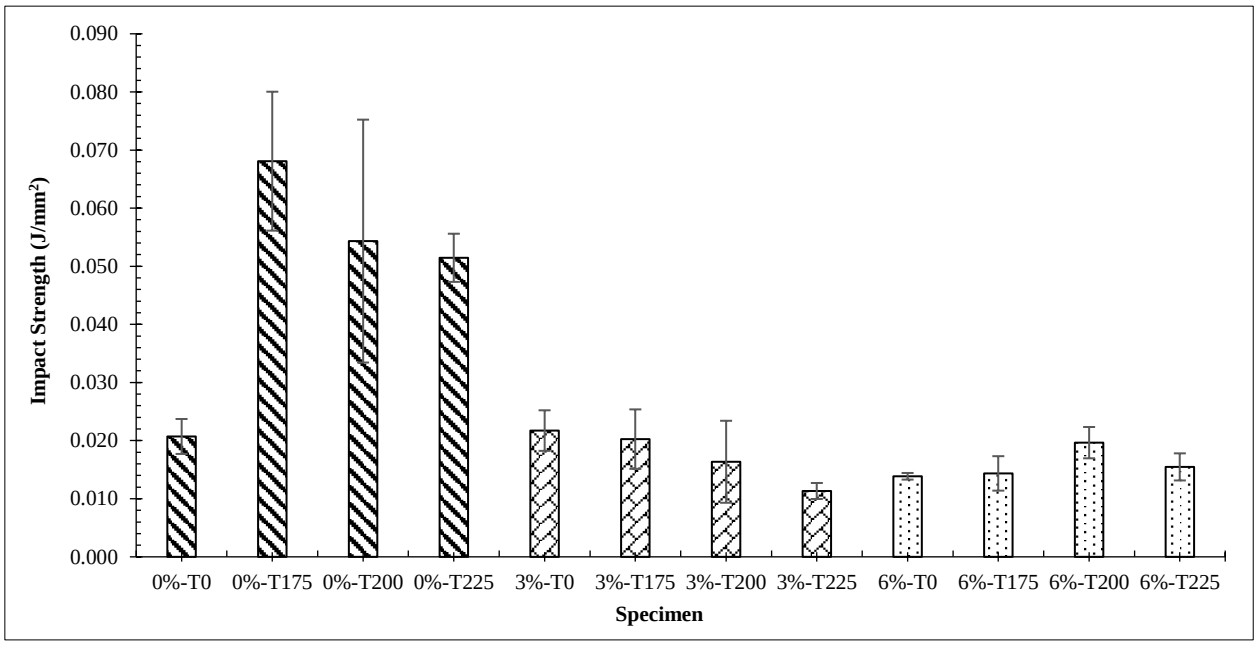

Figure 17. Impact Strength of AA6061–BA composites

The incorporation of 3 wt% and 6 wt% BA reinforcement resulted in a drastic reduction in impact toughness compared to the unreinforced alloy. For the 3 wt% BA condition, the highest value was obtained in the as-cast state (0.0217 J/mm²), while for the 6 wt% BA composite the maximum impact strength was only 0.0196 J/mm² at an aging temperature of 200 °C. The overall low impact toughness in the reinforced composites is likely due to particle agglomeration and increased porosity, which act as preferential sites for crack initiation under dynamic loading. Previous studies on aluminum matrix composites reinforced with fly ash, a material with similar morphology and properties to BA, have shown comparable trends, where reinforcement improved hardness and tensile strength but significantly decreased impact resistance due to brittle fracture mechanisms [53, 54].

Aging treatment also played a key role in determining the fracture behavior of the composites. At 175 °C, the formation of fine Mg_2Si precipitates promoted strengthening without severely compromising toughness, leading to the best balance of mechanical performance in the unreinforced alloy. At higher aging temperatures (200–225 °C), overaged precipitates combined with reinforcement particles contributed to brittle fracture characteristics. The combination of hard BA particles, coarse precipitates, and porosity reduced the material's ability to absorb energy, leading to a sharp drop in impact strength. Furthermore, the presence of brittle Al_5FeSi intermetallic phases exacerbated crack initiation and propagation, further lowering impact toughness in BA-reinforced composites. The results confirm a classic strength–toughness trade-off in heat-treated aluminum composites. The unreinforced alloy achieved the highest impact toughness after aging at 175 °C due to fine precipitation strengthening, whereas the addition of BA reinforcement promoted brittleness and reduced energy absorption capability. These findings highlight the importance of controlling both precipitation behavior and particle distribution to optimize the mechanical response of aluminum matrix composites [49, 50].

These interpretations are further supported by fractography examination of the impact-tested specimens, as illustrated in Figure 18. Numerous tiny dimples on the fracture surface of the unreinforced alloy aged at 175 °C are indicative of ductile fracture and are correlated with the comparatively high absorbed energy. On the other hand,

the 3%wt BA composite showed a heterogeneous morphology, with cleavage facets and signs of particle–matrix interfacial debonding coexisting with areas of tiny dimples. This suggests that although there was some plastic deformation, the BA particles served as stress concentrators, promoting the early onset of cracks. The primarily brittle characteristics of the 6%wt percent BA specimens included wide pores where BA clusters had debonded and flat cleavage planes, which resulted in catastrophic failure with little energy absorption. Similar brittle fractographic features in particle-reinforced aluminum composites have been reported in studies on SiC reinforcements [55], reinforcing the conclusion that higher reinforcement fractions and porosity strongly shift fracture behavior toward brittleness.

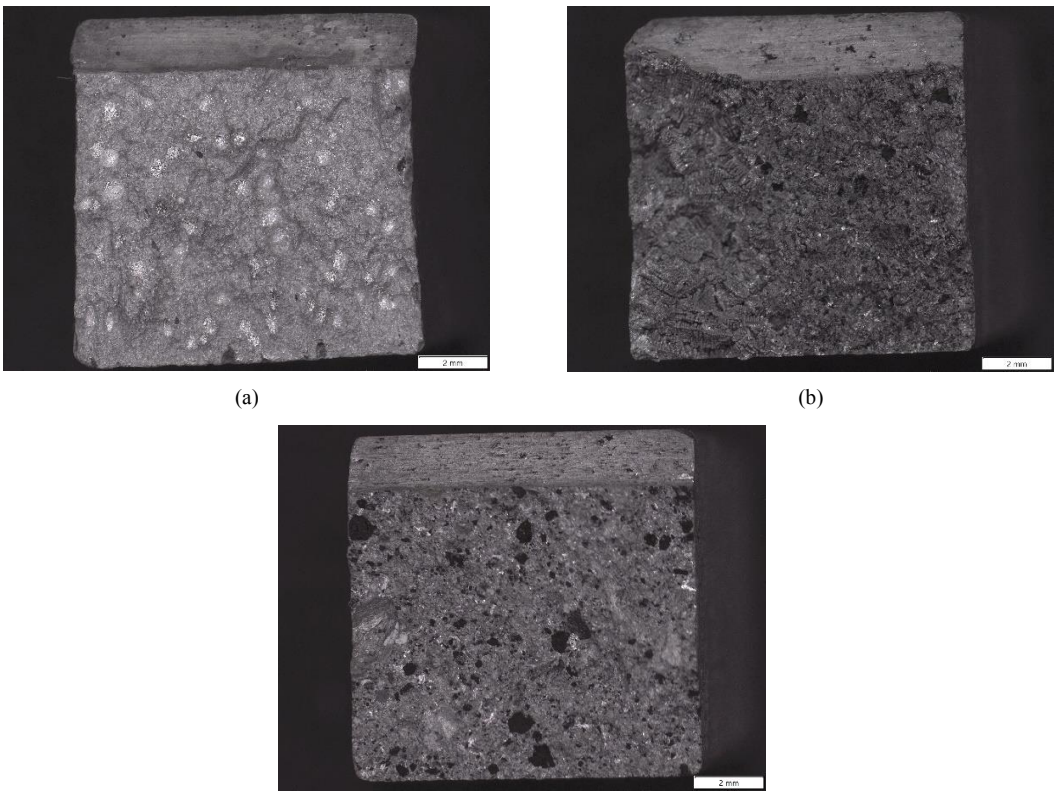

(a) (b)

(c)

Figure 18. Fractography of impact test results (a). 0%wt-T175; (b). 3%wt-T175; (c). 6%wt-T175

3.6. Thermo Mechanical Analysis

The coefficient of thermal expansion (CTE) is a critical parameter for evaluating dimensional stability as temperature changes. The coefficient of thermal expansion (CTE) obtained from thermomechanical analysis (TMA) can be expressed as mean or instantaneous values, each offering distinct insights. The mean CTE represents the average dimensional change over a temperature range, making it useful for predicting overall thermal stability and dimensional reliability in engineering applications. In contrast, the instantaneous CTE reflects the rate of expansion at a specific temperature, providing sensitivity to localized events such as phase transformations, relaxation, or glass transition that are not evident in mean values. Thus, while mean CTE is essential for practical design considerations, instantaneous CTE is valuable for identifying critical thermal responses, and their combined interpretation yields a more comprehensive understanding of material behavior.

In aluminum matrix composites (AMCs), microstructure, reinforcement content, and heat treatment significantly influence thermal expansion behavior. Figures 19 and 20 shows the mean CTE and the instantaneous CTE of AA6061–BA composites respectively. For the unreinforced alloy (0 wt% BA), the mean CTE ranged from approximately 26.67 to 29.42 ppm/K, peaking at the highest aging temperature (T225, 29.42 ppm/K) and reaching its lowest at T200 (26.67 ppm/K), values typical for pure aluminum alloys. Interestingly, the instantaneous CTE in the as-cast (T0) condition was negative (–6.62 ppm/K), indicating localized contraction likely due to residual internal stresses from casting, coarse grains, high porosity, and lack of precipitates (e.g., Mg_2Si). After aging at 175 °C and 200 °C, the instant CTE turned positive (3.18 and 1.42 ppm/K, respectively), reflecting microstructural stabilization via fine precipitate formation. At T225, despite the higher mean CTE, the low instant CTE (1.32 ppm/K) suggests overaging, where coarsened and uneven precipitates reduce local thermal stability.

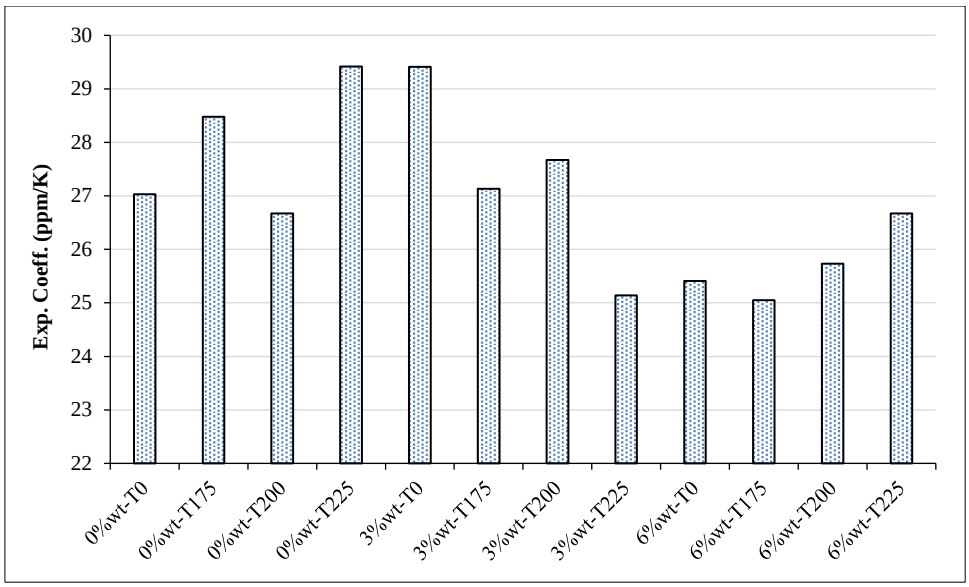

Figure 19. The mean coefficient of thermal expansion (mean-CTE) of AA6061–BA composites

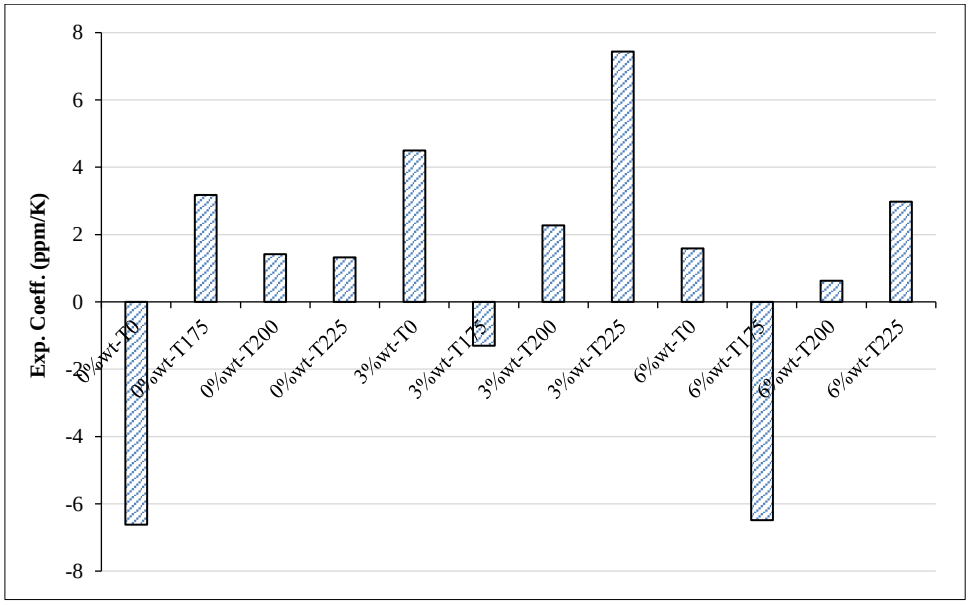

Figure 20. The instant coefficient of thermal expansion (instant-CTE) of AA6061–BA composites

When adding 3 wt% BA, mean CTE values tended to decline compared to the unreinforced alloy (ranging 25.14–29.41 ppm/K), showing that BA, having a much lower CTE than aluminum, effectively restrains overall thermal expansion, consistent with findings in Al–fly ash systems [56] and aluminum composites reinforced with fly ash or SiC, which exhibit decreased CTE [57]. In the as-cast 3 wt% BA sample, the instant CTE was 4.50 ppm/K with the highest mean (29.41 ppm/K), indicating partial stabilization from BA. However, after aging at 175 °C, the instant CTE became negative (–1.30 ppm/K), likely due to non-uniform BA particle distribution or agglomeration creating zones of internal stress and localized contraction. At 200 °C, the instant CTE increased to 2.27 ppm/K and mean dropped to 27.67 ppm/K, suggesting improved homogeneity in the microstructure. At T225, the instant CTE sharply rose to 7.44 ppm/K while the mean decreased to 25.14 ppm/K, signaling uncontrolled local expansion resulting from coarse precipitates and poor interaction between BA particles, confirmed by microstructural observations.

For the 6 wt% BA composite, the mean CTE dropped further to 25.05–26.67 ppm/K, the lowest among all variations, highlighting the efficacy of BA in limiting thermal expansion due to its ceramic nature and low intrinsic CTE. However, instant CTE values remained unstable: at T175, the instant CTE plunged to –6.49 ppm/K, pointing to sudden contraction caused by microstructural instability (BA agglomeration, uneven precipitates). At T0 and T200, the instant CTE was more stable (1.59 and 0.63 ppm/K, respectively), though mean values stayed low (25.41 and 25.73 ppm/K), reflecting a beginning of structural stabilization. At T225, the instant CTE rose to 2.98 ppm/K and the mean reached 26.67 ppm/K, indicating that while overaging occurred, internal microstructural redistribution improved thermal stability relative to lower aging temperatures.

Increasing BA fraction reduced mean CTE, confirming BA's effectiveness in restraining thermal expansion. This trend is consistent with the behavior of ceramic reinforcements such as fly ash, which possess inherently low CTE values and therefore suppress the overall expansion of the aluminum matrix [56]. Instant CTE, however, proved to be more sensitive to microstructural conditions such as residual stresses, particle agglomeration, and precipitate distribution. Negative instant values indicated local instability and contraction due to residual stresses or particle clustering, whereas stable positive values reflected a homogeneous and well-distributed microstructure. The presence of rigid, low-expanding intermetallic phases such as Al_5FeSi also contributed to reducing thermal expansion. Among all conditions, the 3 wt% BA composite aged at 200 °C exhibited the most balanced thermal response, combining reduced mean CTE with stable instant behavior, which points to a uniform microstructure and effective precipitate formation. In contrast, the 6 wt% BA composites achieved the lowest mean CTE values (25.05–26.67 ppm/K), but the unstable instant responses—particularly negative values at 175 °C—revealed severe local instabilities arising from agglomeration and uneven stress distribution.

Overall, the combined analysis of mean and instant CTE highlights that dimensional stability in AA6061–BA composites depends not only on the intrinsic CTE mismatch between matrix and reinforcement but also critically on microstructural uniformity, residual stress relaxation, and the evolution of precipitates during aging. The unreinforced alloy benefited from fine Mg_2Si precipitation at 175 °C, producing stable instant CTE values and improved toughness. With reinforcement, 3 wt% BA at 200 °C provided the most stable condition, whereas 6 wt% BA, despite lowering mean CTE further, suffered from microstructural instabilities that limited its suitability for applications requiring high dimensional precision under thermal cycling. These findings are in strong agreement with Uju & Oguocha [57], who reported that fly ash additions to Al–Mg alloys significantly lowered CTE due to their ceramic nature but also introduced porosity and residual stresses from casting. A more recent study on aluminum–fly ash composites [56] further emphasized that thermal expansion control is governed not only by reinforcement fraction but also by particle distribution, interface bonding, and heat treatment history—factors that directly align with the present observations.

3.7. Coordinate Measuring Machine (CMM)

The Coordinate Measuring Machine (CMM) test was employed to evaluate geometric distortion and dimensional irregularities of the specimens after casting and subsequent heat treatments. The primary parameter assessed was the change in surface area (mm²) along the X-axis and Y-axis for both the top and bottom regions of the specimens (Figure 21). These dimensional variations serve as indicators of thermal instability, residual stress, porosity, and reinforcement particle distribution, all of which reflect the microstructural integrity and thermal expansion behavior of the composites [58].

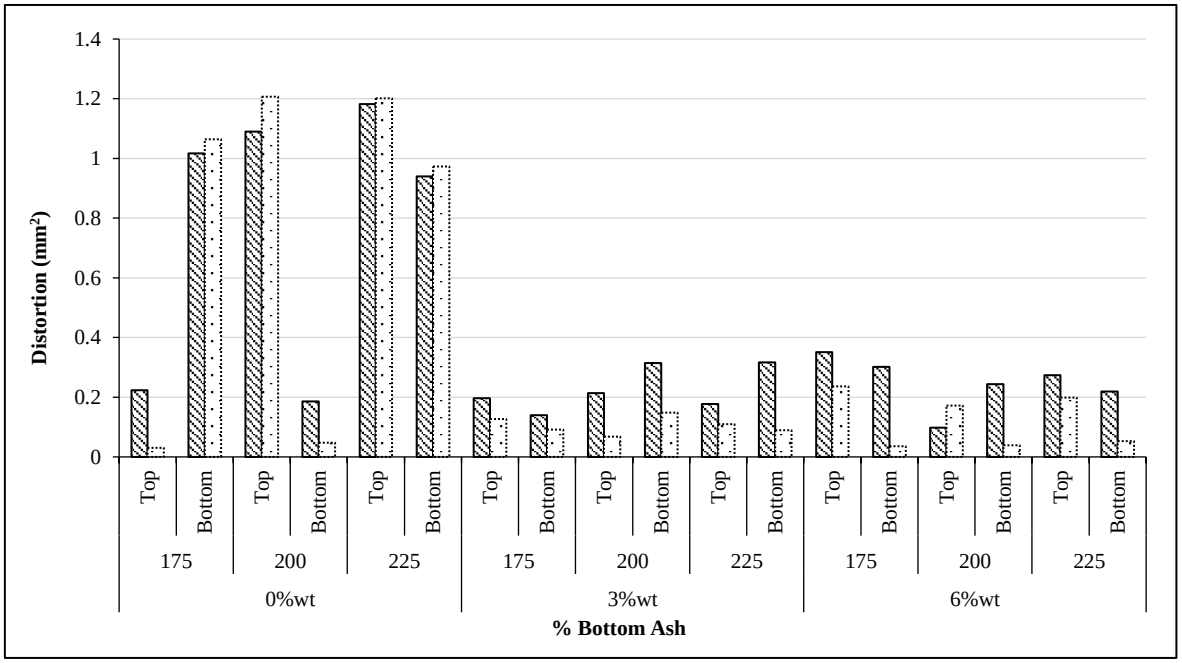

Figure 21. Distortion based on CMM test

For the unreinforced specimens (0%wt bottom ash), Figure 19 reveals a significant increase in surface area distortion, exceeding 1.2 mm² for both the top and bottom sections. This represents the highest distortion across all variations, attributed to the absence of reinforcing particles, which results in low resistance to thermal expansion. Consequently, during the heating and cooling cycles of heat treatment, the specimens underwent severe deformation. These findings

are consistent with TMA results, which indicated that the 0%wt variation had the highest mean coefficient of thermal expansion (29.42 ppm/K). The microstructure under these conditions, particularly after aging at 175 °C and 200 °C, exhibited coarse grains, the absence of hard reinforcement phases, and high porosity. Such features lead to localized thermal expansion. Interestingly, at the T225 condition, the CMM results showed a drastic reduction in distortion (< 0.4 mm²), likely due to microstructural restructuring caused by overaging, where larger precipitates stabilized the matrix and constrained expansion [59].

The addition of 3%wt bottom ash markedly reduced distortion across all measurement points, with values ranging between 0.1–0.4 mm² and only minor fluctuations between the X and Y axes. This indicates symmetrical deformation and high dimensional stability. The 3%wt reinforcement provided a balance of mechanical strengthening and resistance to thermal expansion, consistent with the TMA results that showed a reduced average thermal expansion coefficient (25–27 ppm/K). The microstructure at this composition displayed fine Mg_2Si precipitates and a homogeneous distribution of bottom ash particles, which contributed to uniform thermal and structural responses during heat treatment. The minimal difference between the top and bottom surfaces suggests uniform heat distribution and improved structural reliability. These results indicate that 3%wt bottom ash represents the optimum composition for achieving superior dimensional stability and geometric reliability in the composites.

At the highest reinforcement content (6%wt), the CMM results demonstrated slightly larger distortions compared to 3%wt, accompanied by greater fluctuations between the X and Y axes. Although bottom ash intrinsically has a low thermal expansion coefficient, the high fraction of reinforcement led to particle agglomeration, as confirmed in microstructural observations. Such agglomeration created localized weak zones, disrupted reinforcement continuity, and introduced high internal stresses. This was further supported by TMA results, which revealed negative instantaneous values (e.g., –6.49 ppm/K at T175), indicating sudden contraction and large fluctuations across temperatures. The CMM results showed irregular increases in surface area and significant discrepancies between the top and bottom sections of the specimens, reflecting uneven temperature distribution and microstructural inhomogeneity. Despite the relatively low mean thermal expansion coefficient (25 ppm/K), the instability caused by particle agglomeration and porosity compromised the macroscopic dimensional stability. Therefore, although reinforcement theoretically increases strength, the geometric stability and dimensional reliability at 6%wt reinforcement were less favorable [59, 60].

Overall, the CMM analysis indicates that dimensional stability is not solely determined by reducing global expansion (average CTE), but rather by achieving microstructural homogeneity and controlling residual stresses. The unreinforced alloy was highly unstable due to unconfined expansion, while the 6 wt% BA composite experienced microstructural heterogeneity. The 3 wt% BA composite at 200°C emerged as the most balanced state, combining a reduced average CTE, stable instantaneous response, and minimal CMM distortion. These results underscore the importance of optimizing reinforcement fraction and heat treatment conditions to ensure dimensional reliability in applications requiring tight geometric tolerances, such as aerospace and automotive components.

4. Conclusion

This study comprehensively examined the effect of T6 heat treatment at different aging temperatures and bottom ash (BA) reinforcement on the mechanical performance and dimensional stability of AA6061 composites. The results confirm that aging treatment is a determining factor in microstructure and mechanical properties. The unreinforced alloy achieved the best performance at 175 °C, where ultrafine Mg_2Si precipitates enhanced tensile strength and toughness with stable thermal expansion. The addition of BA particles also reduced the mean coefficient of thermal expansion (CTE), with 3 wt% BA showing the best-balanced performance: it produced smaller overall expansion, lowest CMM distortion, and most stable microstructural response. In contrast, 6 wt% BA, despite yielding the lowest mean CTE, suffered from particle agglomeration, porosity, and residual stresses that destabilized the local microstructure and compromised toughness and dimensional reliability. These results highlight that reinforcement effectiveness depends not only on intrinsic CTE mismatch but also critically on particle distribution, interface bonding, and precipitation evolution during aging.

From a broader perspective, the findings demonstrate that combining controlled heat treatment with moderate BA reinforcement is an effective strategy for improving both mechanical and thermal performance of AA6061-based composites. This approach not only enhances strength, hardness, and dimensional stability but also leverages industrial waste (coal bottom ash) as a sustainable reinforcement material. The dual advantage of mechanical improvement and environmental benefit strengthens the case for BA as a cost-effective alternative to conventional reinforcements. In practical terms, the optimized 3 wt% BA composite aged at 175–200 °C offers a promising material for structural applications that require lightweight components with high dimensional stability under thermal cycling, such as in automotive, aerospace, and civil infrastructure systems. Future studies could focus on long-term thermal fatigue behavior and surface modification of BA to further improve interfacial bonding and minimize porosity, ensuring broader applicability of these sustainable aluminum composites.

5. Declarations

5.1. Author Contributions

Conceptualization, T. and H.S.; methodology, H.S. and S.R.B.; software, D.A.; validation, D.A., E.S., and T.; formal analysis, H.S. and S.R.B.; investigation, S.R.B.; resources, H.S.; data curation, S.R.B.; writing—original draft preparation, H.S. and S.R.B.; writing—review and editing, T.; visualization, S.R.B.; supervision, D.A. and E.S.; project administration, S.R.B.; funding acquisition, H.S. All authors have read and agreed to the published version of the manuscript.

5.2. Data Availability Statement

The data presented in this study are available in the article.

5.3. Funding

The authors received no financial support for the research, authorship, and/or publication of this article.

5.4. Conflicts of Interest

The authors declare no conflict of interest.

6. References

[1] Garg, P., Jamwal, A., Kumar, D., Sadasivuni, K. K., Hussain, C. M., & Gupta, P. (2019). Advance research progresses in aluminium matrix composites: manufacturing & applications. Journal of Materials Research and Technology, 8(5), 4924–4939. doi:10.1016/j.jmrt.2019.06.028.

[2] Ramanathan, A., Krishnan, P. K., & Muraliraja, R. (2019). A review on the production of metal matrix composites through stir casting – Furnace design, properties, challenges, and research opportunities. Journal of Manufacturing Processes, 42, 213–245. doi:10.1016/j.jmapro.2019.04.017.

[3] Bintoro, S. R., Surojo, E., Muhayat, N., & Triyono. (2025). A Comprehensive Review on Fusion Arc Welding of Aluminum Matrix Composites: Challenges, Mechanisms, and Advancements. Results in Engineering, 27, 10625. doi:10.1016/j.rineng.2025.106257.

[4] Li, X., Yan, H., Wang, Z. W., Li, N., Liu, J. L., & Nie, Q. (2019). Effect of heat treatment on the microstructure and mechanical properties of a composite made of Al-Si-Cu-Mg aluminum alloy reinforced with sic particles. Metals, 9(11), 1205. doi:10.3390/met9111205.

[5] Liu, G. F., Chen, T. J., & Wang, Z. J. (2021). Effects of solid solution treatment on microstructure and mechanical properties of SiCp/2024 Al composite: A comparison with 2024 Al alloy. Materials Science and Engineering: A, 817, 141413. doi:10.1016/j.msea.2021.141413.

[6] Zhou, H., Bhattarai, R., Li, Y., Si, B., Dong, X., Wang, T., & Yao, Z. (2022). Towards sustainable coal industry: Turning coal bottom ash into wealth. Science of the Total Environment, 804, 149985. doi:10.1016/j.scitotenv.2021.149985.

[7] Miracle, D. B. (2005). Metal matrix composites – From science to technological significance. Composites Science and Technology, 65(15–16), 2526–2540. doi:10.1016/j.compscitech.2005.05.027.

[8] Harish, T. M., Nandu Krishnan, A. U., Navas, N., & Sreekanth, K. A. (2023). Mechanical and microstructural characterization of aluminium metal matrix composite reinforced with bottom ash and fireclay. Materials Today: Proceedings, 72, 3154–3157. doi:10.1016/j.matpr.2022.10.168.

[9] Beemaraj, R. K., Ramesh, M., Subramaniyan, G. G., & Kamatchi, T. (2024). A study on mechanical and tribological properties of AMMC through stir casting process. Interactions, 245(1), 334. doi:10.1007/s10751-024-02177-5.

[10] Iqbal, A. A., & Amierah, N. (2017). Effect of reinforcement volume fraction on the mechanical properties of the Al-SiC nanocomposite materials. IOP Conference Series: Materials Science and Engineering, 226(1), 12168. doi:10.1088/1757-899X/226/1/012168.

[11] Yuan, Z., Tian, W., Li, F., Fu, Q., Wang, X., Qian, W., & An, W. (2020). Effect of heat treatment on the interface of high-entropy alloy particles reinforced aluminum matrix composites. Journal of Alloys and Compounds, 822, 153658. doi:10.1016/j.jallcom.2020.153658.

[12] Rajkeerthi, E., Satyanarayan, C. P., Jaivignesh, M., Pradeep, N., & Hariharan, P. (2019). Effect of heat treatment on strength of aluminium matrix composites. Materials Today: Proceedings, 46, 4419–4425. doi:10.1016/j.matpr.2020.09.672.

[13] Xu, K., Wang, J., & Zhang, S. (2020). Effect of heat treatment on the microstructure and properties of in-situ Mg2Si reinforced hypereutectic Al-18%Si matrix composites. Materials Research Express, 7(8), 086515. doi:10.1088/2053-1591/abaea2.

[14] Ren, S., Tao, X., Xu, X., Guo, A., Liu, J., Fan, J., ... & Liang, J. (2018). Preparation and characteristic of the fly ash cenospheres/mullite composite for high-temperature application. Fuel, 233, 336-345. doi:10.1016/j.fuel.2018.06.058.

[15] Gong, D., Zhu, M., Cao, Y., Qian, J., Chao, Z., Xiu, Z., & Jiang, L. (2023). Revealing the mechanism of internal stress on dimensional stability in SiC/Al composites under long-term thermal exposure. Vacuum, 209, 111786. doi:10.1016/j.vacuum.2022.111786.

[16] Gong, D., Cao, Y., Chao, Z., Xiu, Z., & Jiang, L. (2022). Revealing the Effect of Internal Stress on Dimensional Stability of Sic/Al Composites under Long-Term Thermal Exposure. SSRN Electronic Journal, 1-27. doi:10.2139/ssrn.4170559.

[17] Kumar, R., Bairwa, K. N., Vemanaboina, H., Naidu, B. V. V., Shoush, K. A., Pushkarna, M., Tuka, M. B., & Ghoneim, S. S. M. (2024). Enhancing wear resistance of aluminum 6061 composites with fly ash: A sustainable approach for industrial applications. Advances in Mechanical Engineering, 16(10), 1–11. doi:10.1177/16878132241290913.

[18] Ravichandran, M., Balasubramanian, M., Anand Chairman, C., Marichamy, S., Dhinakaran, V., & Stalin, B. (2020). Mechanical properties of Fly ash reinforced Aluminium matrix composites. IOP Conference Series: Materials Science and Engineering, 988(1), 12095. doi:10.1088/1757-899X/988/1/012095.

[19] Muhardi, A., Marto, A., Kassim, K. A., Makhtar, A. M., Wei, L. F., & Lim, Y. S. (2010). Engineering characteristics of Tanjung Bin coal ash. Electronic Journal of Geotechnical Engineering, 15 K, 1117–1129.

[20] Krishnakumar, M., Hariharan, J., & Saravanan, R. (2019). Effect on distribution of siderite on aluminium-7% silicon alloy by stir casting. Materials Today: Proceedings, 27, 2418–2423. doi:10.1016/j.matpr.2019.09.202.

[21] Patil, C. S., Ansari, M. I., Selvan, R., & Thakur, D. G. (2021). Influence of micro B4C ceramic particles addition on mechanical and wear behavior of aerospace grade Al-Li alloy composites. Sādhanā, 46(1), 11. doi:10.1007/s12046-020-01543-7.

[22] Rajasekaran, S., Udayashankar, N. K., & Nayak, J. (2012). T4 and T6 Treatment of 6061 Al-15 Vol. % SiC P Composite. ISRN Materials Science, 2012, 1–5. doi:10.5402/2012/374719.

[23] Shankar, K. V., Jezierski, J., Ramalingam, V. V., Padmakumar, D., Leena, M. R., Amal, A., Reghunath, G., & Krishnan, R. (2022). Investigating the Effect of Fly Ash Addition on the Metallurgical and Mechanical Behavior of Al-Si-Mg-Cu Alloy for Engine Cylinder Head Application. Materials, 15(15), 5462. doi:10.3390/ma15155462.

[24] Juang, S. H., & Li, C. F. (2022). Influence of Different Addition Ratios of Fly Ash on Mechanical Properties of ADC10 Aluminum Matrix Composites. Metals, 12(4), 653. doi:10.3390/met12040653.

[25] Herman, A. P., Yusup, S., Shahbaz, M., & Patrick, D. O. (2016). Bottom Ash Characterization and its Catalytic Potential in Biomass Gasification. Procedia Engineering, 148, 432–436. doi:10.1016/j.proeng.2016.06.447.

[26] Das, D. K., Mishra, P. C., Singh, S., & Thakur, R. K. (2014). Properties of ceramic-reinforced aluminium matrix composites- A review. International Journal of Mechanical and Materials Engineering, 9(1), 12. doi:10.1186/s40712-014-0012-9.

[27] Sharma, S. K., Gajević, S., Sharma, L. K., Pradhan, R., Sharma, Y., Miletić, I., & Stojanović, B. (2024). Progress in Aluminum-Based Composites Prepared by Stir Casting: Mechanical and Tribological Properties for Automotive, Aerospace, and Military Applications. Lubricants, 12(12), 421. doi:10.3390/lubricants12120421.

[28] Sharma, V. K., Singh, R. C., & Chaudhary, R. (2017). Effect of flyash particles with aluminium melt on the wear of aluminium metal matrix composites. Engineering Science and Technology, an International Journal, 20(4), 1318–1323. doi:10.1016/j.jestch.2017.08.004.

[29] Razzaq, A. M., Majid, D. L., Ishak, M. R., & Basheer, U. M. (2017). Effect of fly ash addition on the physical and mechanical properties of AA6063 alloy reinforcement. Metals, 7(11), 477. doi:10.3390/met7110477.

[30] Kareem, A., Qudeiri, J. A., Abdudeen, A., Ahammed, T., & Ziout, A. (2021). A review on AA 6061 metal matrix composites produced by stir casting. Materials, 14(1), 1–22. doi:10.3390/ma14010175.

[31] Zulfia, A., Ramdaniawati, D., & Dhaneswara, D. (2018). The Role of Al2O3 Nanoparticles Addition on Characteristic of Al6061 Composite Produced by Stir Casting Process. International Journal of Materials Science and Engineering, 6(2), 39–47. doi:10.17706/ijmse.2018.6.2.39-47.

[32] Zhu, H., Guo, G., Cui, T., Huang, J., Li, J., & Xie, Z. (2015). Influences of carbon additions on reaction mechanisms and tensile properties of Al-based composites synthesized in-situ by Al-SiO2 powder system. Materials Science and Engineering: A, 623, 78–82. doi:10.1016/j.msea.2014.11.043.

[33] Liu, K., Mirza, F. A., & Chen, X. G. (2018). Effect of overaging on the cyclic deformation behavior of an AA6061 aluminum alloy. Metals, 8(7), 528. doi:10.3390/met8070528.

[34] DiCecco, S., Di Ciano, M., Baghbanaghaie, N., Esmaeili, S., Wells, M. A., & Worswick, M. J. (2023). Warm Aging of Pre-aged AA6013 Sheet and Its Relevance to Room Temperature and Warm Forming Applications—Experimental and Modeling Analyses. Journal of Materials Engineering and Performance, 32(21), 9797–9813. doi:10.1007/s11665-023-08216-6.

[35] Siddesh Kumar, N. M., Dhruthi, Pramod, G. K., Samrat, P., & Sadashiva, M. (2022). A Critical Review on Heat Treatment of Aluminium Alloys. Materials Today: Proceedings, 58, 71–79. doi:10.1016/j.matpr.2021.12.586.

[36] Dwivedi, S. P., Srivastava, A. K., Maurya, N. K., & Maurya, M. (2019). Microstructure and mechanical properties of Al 6061/Al2O3/Fly-Ash composite fabricated through stir casting. Annales de Chimie: Science Des Materiaux, 43(5), 341–348. doi:10.18280/acsm.430510.

[37] Singh, B., Grewal, J. S., & Sharma, S. (2021). Effect of addition of flyash and graphite on the mechanical properties of A6061-T6. Materials Today: Proceedings, 50, 2411–2415. doi:10.1016/j.matpr.2021.10.258.

[38] Razzaq, A. M., Majid, D. L., Basheer, U. M., & Aljibori, H. S. S. (2021). Research summary on the processing, mechanical and tribological properties of aluminium matrix composites as effected by fly ash reinforcement. Crystals, 11(10), 1212. doi:10.3390/cryst11101212.

[39] Kumar, S., Bera, S., Mandal, D., & Chakraborty, A. K. (2025). Transforming waste red mud and fly ash to wealth by designing a hybrid Al alloy composite with improved mechanical and tribological properties. Materialwissenschaft Und Werkstofftechnik, 56(1), 122–131. doi:10.1002/mawe.202300378.

[40] Medvecká, D., Kuchariková, L., & Uhríčik, M. (2020). The failure degradation of recycled aluminium alloys with high content of β-al5fesi intermetallic phases. Defect and Diffusion Forum, 403 DDF, 97–102. doi:10.4028/www.scientific.net/DDF.403.97.

[41] Mathew, J., Remy, G., Williams, M. A., Tang, F., & Srirangam, P. (2019). Effect of Fe Intermetallics on Microstructure and Properties of Al-7Si Alloys. JOM, 71(12), 4362–4369. doi:10.1007/s11837-019-03444-5.

[42] Shetty, A., Bhat, T., Sharma, S., Hegde, A., K, N., Prabhu, R., & Anne, G. (2025). Effects of Magnesium Content and Age Hardening Parameters on the Hardness and Ultimate Tensile Strength of SiC-Reinforced Al-Si-Mg Composites. Journal of Composites Science, 9(1), 5. doi:10.3390/jcs9010005.

[43] Hegde, A., Birur Manjunathaiah, K., Sharma, S., Mandya Chennegowda, G., Anne, G., & Sadanand, R. V. (2024). Hybrid Treatment and Natural Aging Behavior of Peak-Aged Eutectoid Steel Powder-Reinforced Al 7075 Matrix Composites. Journal of Composites Science, 8(3), 89. doi:10.3390/jcs8030089.

[44] Madhusudan, S., Sarcar, M. M. M., & Rao, N. B. R. M. (2016). Mechanical properties of Aluminum-Copper(p) composite metallic materials. Journal of Applied Research and Technology, 14(5), 293–299. doi:10.1016/j.jart.2016.05.009.

[45] Doddamani, S., & Kaleemulla, M. (2019). Effect of graphite on fracture toughness of 6061Al-graphite. Strength, Fracture and Complexity, 11(4), 295–308. doi:10.3233/sfc-180230.

[46] Rong, X., Chen, X., Zhao, D., Zhang, X., He, C., Shi, C., & Zhao, N. (2023). Effect of aging treatment on microstructure and mechanical properties of Al matrix composite reinforced by in-situ intragranular Al2O3. Materials Characterization, 204, 113215. doi:10.1016/j.matchar.2023.113215.

[47] Das, D., Samal, C., Chaubey, A. K., & Nayak, R. K. (2019). Influence of thermal treatment and reinforcement content on properties of aluminium matrix composites: A case study. Materials Today: Proceedings, 18, 3262–3267. doi:10.1016/j.matpr.2019.07.202.

[48] Cheneke, S., & Benny Karunakar, D. (2019). The effect of solution treatment on aging behavior and mechanical properties of AA2024-TiB2 composite synthesized by semi-solid casting. SN Applied Sciences, 1(11), 1501. doi:10.1007/s42452-019-1531-z.

[49] Liu, F., Yu, F., & Zhao, D. (2022). Aging Behavior and Precipitates Analysis of Wrought Al-Si-Mg Alloy. Materials, 15(22), 8194. doi:10.3390/ma15228194.

[50] Meyruey, G., Massardier, V., & Perez, M. (2020). Aging of an Al-Mg-Si Alloy with a Silicon Excess and Reinforced with Ceramic Particles. Metallurgical and Materials Transactions A, 51(6), 3124–3141. doi:10.1007/s11661-020-05736-x.

[51] Jiang, G. D., Cai, Y. H., Qiu, C., Zhang, W. W., & Zhang, D. T. (2022). Effect of over-aging on the microstructure, mechanical properties and crashing performance of thin-walled Al-Mg-Si-Cu alloy profiles. Journal of Materials Research and Technology, 21, 3074–3085. doi:10.1016/j.jmrt.2022.10.137.

[52] Ahmadian, H., Zhou, T., Alansari, A., Kumar, A. S., Fathy, A., Elmahdy, M., Yu, Q., & Weijia, G. (2024). Microstructure, mechanical properties and wear behavior of Mg matrix composites reinforced with Ti and nano SiC particles. Journal of Materials Research and Technology, 31, 4088–4103. doi:10.1016/j.jmrt.2024.07.125.

[53] Liu, L., Hou, Y., Ye, T., Zhang, L., Huang, X., Gong, Y., Liu, C., Wu, Y., & Duan, S. (2024). Effects of Aging Treatments on the Age Hardening Behavior and Microstructures in an Al-Mg-Si-Cu Alloy. Metals, 14(2), 238. doi:10.3390/met14020238.

[54] Tang, H. P., Wang, Q. D., Luo, C., Lei, C., Liu, T. W., Li, Z. Y., Jiang, H. Y., Ding, W. J., Fang, J., & Zhang, J. W. (2020). Effects of aging treatment on the precipitation behaviors and mechanical properties of Al-5.0Mg-3.0Zn-1.0Cu cast alloys. Journal of Alloys and Compounds, 842, 155707. doi:10.1016/j.jallcom.2020.155707.

[55] Vasanth Kumar, H. S., Revanna, K., Kumar, N., Sathyanarayana, N., Madeva, N., Manjunath, G. A., & Adisu, H. (2022). Impact of Silicon Carbide Particles Weight Percentage on the Microstructure, Mechanical Behaviour, and Fractography of Al2014 Alloy Composites. Advances in Materials Science and Engineering, 2839150, 10. doi:10.1155/2022/2839150.

[56] Nordin, S. S., Mhd Noor, E. E., & Chockalingam, P. (2024). Chemical and Thermal Analysis of Fly Ash-Reinforced Aluminum Matrix Composites (AMCs). Journal of Composites Science, 8(5), 170. doi:10.3390/jcs8050170.

[57] Uju, W. A., & Oguocha, I. N. A. (2012). A study of thermal expansion of Al-Mg alloy composites containing fly ash. Materials and Design, 33(1), 503–509. doi:10.1016/j.matdes.2011.04.056.

[58] Chen, G. Q., Xiu, Z. Y., Yang, W. S., Jiang, L. T., & Wu, G. H. (2010). Effect of thermal-cooling cycle treatment on thermal expansion behavior of particulate reinforced aluminum matrix composites. Transactions of Nonferrous Metals Society of China (English Edition), 20(11), 2143–2147. doi:10.1016/S1003-6326(09)60432-5.

[59] Fu, L., Wu, G., Zhou, C., Xiu, Z., Yang, W., & Qiao, J. (2021). Effect of microstructure on the dimensional stability of extruded pure aluminum. Materials, 14(17), 4797. doi:10.3390/ma14174797.

[60] Xiao, L. R., Tu, X. X., Zhao, X. J., Cai, Z. Y., & Song, Y. F. (2020). Microstructural evolution and dimensional stability of TiC-reinforced steel matrix composite during tempering. Materials Letters, 259, 126871. doi:10.1016/j.matlet.2019.126871.